

1
2
3
4
5
6
7
8
9
10
11
12
13
14
15
16
17
18
19
20
21
22
23

Using Multi-Homologue Plant-Wax Carbon Isotope Signatures to Reconstruct Tropical Vegetation Types

C. Häggi^{1*}, D. J. Bertassoli Jr.^{2,3}, T. K. Akabane³, R. T. So¹, A. O. Sawakuchi³, C. M. Chiessi³, V. R. Mendes⁴, C. A. Jaramillo⁵, S. J. Feakins¹

¹ Department of Earth Sciences, University of Southern California, 3651 Trousdale Pkwy, Los Angeles CA-90089, USA

² School of Arts, Sciences and Humanities, University of São Paulo, Av. Arlindo Bettio 1000, 03828-000 São Paulo SP, Brazil

³ Institute of Geosciences, University of São Paulo, Rua do Lago 562, 05508-080 São Paulo SP, Brazil

⁴ Institute of Marine Science, Federal University of São Paulo, Rua Dr. Carvalho de Mendonça 144, Santos 110-070, Brazil

⁵ Smithsonian Tropical Research Institute, Apartado 0843-03092, Balboa, Ancón, Panama

Corresponding author: Christoph Häggi (christoph.haeggi@gmx.ch)

*Now at: Intercantonal Laboratory Schaffhausen, Mühlentalstrasse 188, 8200 Schaffhausen, Switzerland

Key Points:

- 24 • *n*-Alkane and fatty acid carbon isotope compositions were studied to provide proxy
25 endmembers for tropical South American vegetation types
- 26 • Forest vegetation types show a narrow carbon isotope range facilitating the detection of
27 minor savanna incursions into rainforest
- 28 • The offset of the carbon isotope composition of different *n*-alkane homologues can be
29 used to differentiate savannas and shrublands
30

31 **Abstract**

32 The stable carbon isotope composition ($\delta^{13}\text{C}$) of plant components such as plant wax biomarkers
33 is an important tool for reconstructing past vegetation. Plant wax $\delta^{13}\text{C}$ is mainly controlled by
34 photosynthetic pathways, allowing for the differentiation of C_4 tropical grasses and C_3 forests.
35 Proxy interpretations are however complicated by additional factors such as aridity, vegetation
36 density, elevation, and the considerable $\delta^{13}\text{C}$ variability found among C_3 plant species.
37 Moreover, studies on plant wax $\delta^{13}\text{C}$ in tropical soils and plants have focused on Africa, while
38 structurally different South American savannas, shrublands and forests remain understudied.
39 Here, we analyze the $\delta^{13}\text{C}$ composition of long-chain *n*-alkanes and fatty acids from tropical
40 South American soils and leaf litter to assess the isotopic variability in each vegetation type and
41 to investigate the influence of climatic features on $\delta^{13}\text{C}$. Rainforests and open vegetation types
42 show distinct values, with rainforests having a narrow range of low $\delta^{13}\text{C}$ values (*n*- C_{29} *n*-alkane:
43 $-34.5^{+0.9}_{-0.6}\text{‰}$ (Q_{25}^{75}); Suess-effect corrected) allowing for the detection of even minor incursions
44 of savanna into rainforests (^{13}C -enriched). While Cerrado savannas and semi-arid Caatinga
45 shrublands grow under distinctly different climates, they can yield indistinct $\delta^{13}\text{C}$ values for most
46 compounds. Cerrado soils and litter show pronounced isotopic spreads between the *n*- C_{33} and *n*-
47 C_{29} alkanes, while Caatinga shrublands show consistent values across the two homologues,
48 thereby enabling the differentiation of these vegetation types. The same multi-homologue isotope
49 analysis can be extended to differentiate African shrublands from savannas.

50

51 **Plain Language Summary**

52 The reconstruction of past vegetation dynamics is key for the understanding of the impact of
53 future climate variability on ecosystems. One of the most widely used tools to reconstruct past
54 vegetation from sediment deposits are plant waxes – comparably stable molecules that form the
55 wax coating of leaves. The ratio of heavier and lighter carbon isotopes preserved in plant waxes
56 can be used to differentiate between rainforest and tropical savanna vegetation. This method has
57 been frequently applied in African vegetation types. Other tropical regions such as South
58 America, which have different vegetation structure, remain understudied. In our study, we
59 characterize the plant wax carbon isotope composition of the major tropical South American

60 vegetation types. One of the complications of the method in both African and South American
61 vegetation types is that (semi-) arid shrublands and savannas show similar plant wax carbon
62 isotope values. To further differentiate between arid shrublands and savannas, we show that the
63 comparison of the carbon isotope values from different plant waxes can be useful both in Africa
64 and South America.

65

66 **1. Introduction**

67 Tropical South America is home to diverse tropical vegetation types such as the Amazon and
68 Atlantic rainforests, the Cerrado savanna, the Llanos savanna and the Caatinga shrublands,
69 which include the most biodiverse rainforest and savanna biomes on Earth (Jenkins et al., 2013;
70 Kier et al., 2009). Reconstructions of past tropical vegetation dynamics are essential to
71 understand both the sensitivity of tropical vegetation types to climate variability and the origin of
72 regional biodiversity (Brienen et al., 2015; Cox et al., 2013; Häggi et al., 2017; Salati et al.,
73 1979; Zemp et al., 2017). Aside from the study of plant microfossils (pollen and phytoliths) in
74 sedimentary archives, the main tool used in these reconstructions is the carbon isotope
75 composition ($\delta^{13}\text{C}$) of plant organic matter (Cerling et al., 2011; Feakins et al., 2013; Huang et
76 al., 2000; Schefuß et al., 2005). This approach is based on the different carbon fixation
77 mechanisms used by tropical forest and grass species. While most plants, including tropical
78 forest species, use the C_3 metabolism that involves direct carbon fixation through the Calvin
79 cycle, the C_4 metabolism has an added additional step of pre-concentration of CO_2 through the
80 Hatch-Slack cycle prior to fixation via the Calvin cycle (Kortschak et al., 1965; Slack & Hatch,
81 1967). The C_3 pathway discriminates against the heavy isotope ^{13}C , preferentially taking up ^{12}C .
82 Due to the higher efficiency of carbon fixation by C_4 metabolism, heavy isotope discrimination
83 is less pronounced in C_4 plants, which leads to contrasting stable carbon isotope compositions in
84 plant organic matter from tropical grasses and trees (O'Leary, 1981; Rieley et al., 1991).

85

86 The $\delta^{13}\text{C}$ compositions of soil organic matter, soil carbonates and tooth enamel have been widely
87 used for reconstructions of past vegetation from terrestrial settings (Cerling et al., 1997; Cerling
88 et al., 2011). The $\delta^{13}\text{C}$ composition of refractory plant components such as plant wax biomarkers
89 can also be used for applications in marine, lacustrine and aeolian sediment archives that
90 integrate a larger catchment (Huang et al., 2001; W. Liu et al., 2005; Schefuß et al., 2005). The

91 most commonly used plant wax biomarkers are long-chain *n*-alkanes and long-chain fatty acids
92 that form the wax coating of leaves (Eglinton & Hamilton, 1967) and their isotope compositions
93 remains stable during deposition and post depositional degradation (Häggi et al., 2021). During
94 their synthesis, fractionation yields lower $\delta^{13}\text{C}$ values than bulk organic matter (Collister et al.,
95 1994; Rieley et al., 1991). Detailed studies on the $\delta^{13}\text{C}$ composition of plant wax homologues of
96 varying chain lengths from individual C_3 and C_4 species found a larger range of isotope values
97 for C_3 plants than for C_4 plants (Boom et al., 2014; Garcin et al., 2014; Krull et al., 2006;
98 Rommerskirchen et al., 2006; Vogts et al., 2009; Wu et al., 2017). In addition to the dominant
99 impact of the photosynthetic metabolism, climate conditions and altitude have been found to act
100 as secondary forcing mechanisms controlling plant wax $\delta^{13}\text{C}$ compositions, with aridity and
101 higher altitudes leading to higher $\delta^{13}\text{C}$ values (Ceccopieri et al., 2021; Diefendorf et al., 2010;
102 Wu et al., 2017).

103

104 The $\delta^{13}\text{C}$ composition of plant waxes has also been studied in soils, as well as in marine and
105 lacustrine sediments covering gradients between tree-dominated and grass-dominated vegetation.
106 In mixed vegetation types, the *n*- C_{29} *n*-alkane, produced in large concentrations by tropical trees,
107 yields lower $\delta^{13}\text{C}$ values values than the *n*- C_{31} and *n*- C_{33} *n*-alkanes evenly produced by both trees
108 and grasses (Douglas et al., 2012; Garcin et al., 2014; Rommerskirchen et al., 2003; Schwab et
109 al., 2015; D. Zhang et al., 2021). Hence, the $\delta^{13}\text{C}$ composition of *n*- C_{29} is particularly sensitive to
110 limited tree vegetation in a grass-dominated, while the $\delta^{13}\text{C}$ of *n*- C_{33} can better detect limited
111 grass expansions in a forest-dominated biome (Garcin et al., 2014). The study of multiple plant
112 wax homologues has thereby the potential to elucidate the vegetation structure in greater detail
113 than the $\delta^{13}\text{C}$ of bulk organic matter. The variance in the isotope composition of plant waxes of
114 different chain-length has also been suggested as a tool for assessing past plant biodiversity
115 (Magill et al., 2019). Calibration studies on plant wax biomarker $\delta^{13}\text{C}$ from tropical savanna and
116 forest areas have so far focused on Africa and there are only few other studies from Central
117 America (Douglas et al., 2012) and northern Australia (Krull et al., 2006). There are, however,
118 no systematic studies on the savanna and shrubland vegetation types of tropical South America.

119

120 South American savanna vegetation types show marked differences to African and Australian
121 counterparts. For instance, they exist under more humid climate conditions than African and

122 Australian savannas and evolved different responses to fire and herbivory disturbances (Dantas
123 & Pausas, 2013; Hirota et al., 2011; Lehmann et al., 2014). This resulted in a pattern where
124 African savanna vegetation features higher stems more adapted to herbivory disturbance, while
125 South American savanna vegetation has thicker bark as an adaptation to high fire activity
126 (Dantas & Pausas, 2013; Lehmann et al., 2014). The unique vegetation structure of the South
127 American Cerrado savanna and Caatinga shrubland and the lack of plant-wax isotope data from
128 these vegetation types presents a knowledge gap that has implications for the accurate
129 interpretation of plant wax signals recorded in marine, lacustrine and riverine sediment cores
130 from the region (Bertassoli et al., 2019; Ferreira et al., 2022; Fornace et al., 2016; Häggi et al.,
131 2017; Mulitza et al., 2017; Reis et al., 2022).

132
133 In tropical South America, the study of the $\delta^{13}\text{C}$ composition of plant waxes in leaf, soil and
134 fluxival sediment samples has focused on the Amazon rainforest. On a transect across the Andes-
135 Amazon, Wu et al. (2017), found a trend towards higher $\delta^{13}\text{C}$ values with increasing altitude.
136 The transport of plant wax compounds and their $\delta^{13}\text{C}$ values has been studied in a broader area
137 covering the Amazon River main stem and some of its tributaries (Bertassoli et al., 2022;
138 Feakins et al., 2018; Häggi et al., 2016). The study of plant waxes derived from open vegetation
139 types is so far limited to marine sediments offshore the Caatinga shrubland in northeastern
140 Brazil, where long-chain *n*-alkane $\delta^{13}\text{C}$ values were higher than in the Amazon plume (Häggi et
141 al., 2016). Yet, there is no detailed information on the $\delta^{13}\text{C}$ composition of plant waxes from
142 different savanna and shrubland vegetation types in tropical South America.

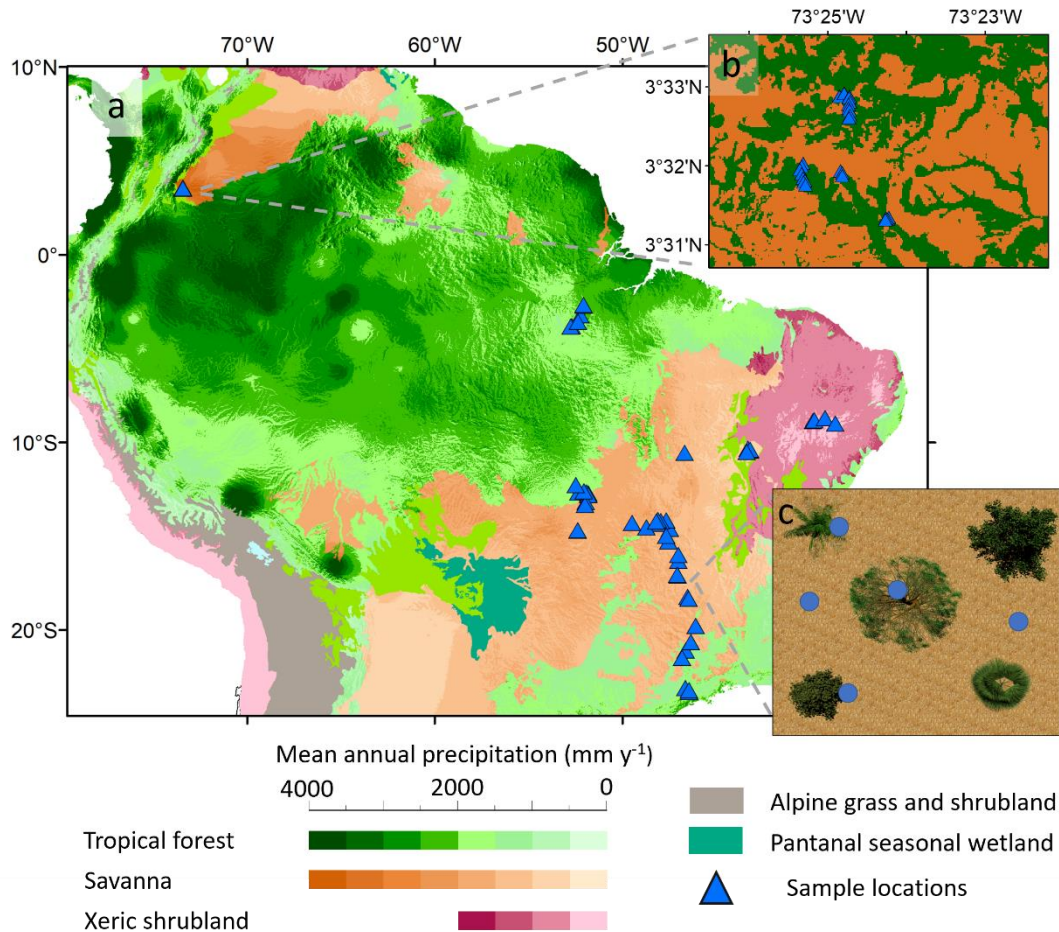
143
144 To fill this gap, we studied the $\delta^{13}\text{C}$ composition of long-chain *n*-alkanes, long-chain fatty acids
145 and bulk organic matter from leaf-litter and soil samples across all major vegetation types of
146 tropical South America, including the Amazon and Atlantic rainforests, the Cerrado savanna, the
147 Caatinga shrubland and the savannas and riparian forests of the Llanos. We first assess the
148 relative distribution of plant wax homologues, to test if assumptions on different distributions
149 between C_3 and C_4 plants observed elsewhere also hold in tropical South America. We then
150 report the $\delta^{13}\text{C}$ endmember values of the different tropical South American vegetation types.
151 Finally, we use the $\delta^{13}\text{C}$ composition of plant wax homologues of different chain-length to

152 further assess differences between South American savanna and shrubland vegetation types and
 153 compare our findings to African tropical vegetation.

154

155 2. Materials and methods

156 2.1. Study area



157

158 **Figure 1.** Study area and sampling strategy. a) Vegetation and precipitation map of tropical
 159 South America (Karger et al., 2017; Olson et al., 2001). Coloring indicates the major biomes of
 160 tropical South America (Olson et al., 2001), while color shades represent mean annual
 161 precipitation (MAP). Note the separate shading for each biome. Sample locations are given in
 162 blue triangles. b) Close-up view of the sampling strategy in the Llanos where transects over the
 163 savanna-riparian forest mosaic were studied. c) Schematic overview of how the five samples at
 164 each site in the Cerrado savanna were taken in proximity to trees, shrubs and grasses.

165

166 The study area covers all major biomes in tropical South America including the Atlantic
167 rainforest, the Amazon rainforest, the Cerrado savanna types of varying tree density, the Llanos
168 savanna and the Caatinga shrubland. The Atlantic rainforest can be found along the eastern coast
169 of South America (Fig. 1) extending from temperate to tropical latitudes, and consists of a humid
170 rainforest vegetation that becomes gradually drier inland, where it merges into Cerrado savanna
171 vegetation (De Azevedo, 1950; Oliveira-Filho & Fontes, 2000). The areas close to the equator
172 between 10°S and 5°N are mostly covered by the Amazon rainforest (Fig. 1). The most humid
173 parts of the Amazon rainforest are found in the northwestern parts of the Amazon Basin, while in
174 the south and east less humid conditions persist (Karger et al., 2017). Cerrado spreads between
175 the Amazon and the Atlantic rainforests and consists of a continuum of savanna vegetation of
176 varying density (Fig. S1) (da Silva & Bates, 2002). The densest physiognomic variety is the
177 Cerradão, which is a dry forest vegetation type that contains little to no grasses (Eiten, 1972).
178 The Cerrado sensu stricto is a mixed savanna with trees and interspersed grasses (Goodland,
179 1971). The Campo Cerrado is a more open Cerrado variety with fewer trees and shrubs that are
180 smaller in size than in Cerrado sensu stricto (Goodland, 1971). The open most varieties are
181 Campo Sujo and Campo Limpo, which are open grass-dominated vegetation types that contain at
182 most a few small shrubs (Goodland, 1971). The distribution of these Cerrado physiognomies
183 depends on proximity to rivers and creeks and on soil properties that define water availability
184 through the dry season (Ruggiero et al., 2002). To the north of the Amazon Basin (3 to 7°N), the
185 Llanos savanna stretches between the Andes and the mouth of the Orinoco River (Fig. 1). The
186 Llanos is also made up of a variety of different types of varying tree density (Blydenstein, 1967).
187 The Llanos also contains the Riparian Forest, a type of forest that is only found along the river
188 margins and represents a subset of the Amazonian Rainforest where water is available all year
189 long via water-table (Jaramillo, 2023). Caatinga shrubland vegetation (also called xerophytic
190 forest) is found in northeastern Brazil and constitutes the driest of the studied vegetation types
191 (Fig. 1). Caatinga vegetation is mostly made up of deciduous shrubs and trees but never with a
192 continuous canopy, as well as succulents and grasses (da Silva & Lacher, 2020; de Queiroz,
193 2006). In contrast to the Cerrado vegetation types, understory grass cover is less dense and
194 sometimes absent from Caatinga shrublands (Lloyd et al., 2008).

195

196 Mean annual precipitation (MAP) in the study area varies between 500 mm y⁻¹ in the Caatinga of
197 northeastern Brazil and 3500 mm y⁻¹ in the northwestern Amazon and the Llanos Basin (Fig. 1)
198 (Karger et al., 2017). While Caatinga shrublands are characterized by distinctly lower
199 precipitation values than the surrounding Cerrado savanna, the boundary between the Llanos
200 savanna and the Amazon rainforest in the northern portion of the continent features continuously
201 high MAP values (Fig. 1). Rather than on MAP, the boundary between Llanos savanna and
202 rainforest is heavily dependent on the duration of wet spells during the dry season (Hoyos et al.,
203 2022). Likewise, the boundary between the Cerrado and the drier southern part of the Amazon
204 rainforest is also not defined by a distinct MAP boundary (Fig. 1).

205

206 Mean annual temperatures vary between 18 °C in portions of the Atlantic rainforest areas and 27
207 °C in the Caatinga shrublands (Karger et al., 2017). The Caatinga shrubland, therefore, features
208 both the warmest and driest conditions in the study area. The low temperatures in the Atlantic
209 rainforest sites are related to its latitudinal position and elevated altitude in the mountainous
210 areas of southeastern Brazil.

211

212 **2.2.Sampling**

213 Soil and leaf litter samples were collected during three field campaigns to the different South
214 American vegetation types (Häggi, Naafs, et al., 2023). Soil samples consist of the upper five
215 centimeters of the A-horizon, while leaf litter samples consist of loose-leaf material found on top
216 of the sampled soils. Samples from the Atlantic rainforest, the Cerrado, and the southern
217 Amazon rainforest were collected in April 2019. Sampling was conducted on sites featuring
218 undisturbed primary vegetation. Special care was taken to avoid locations where invasive species
219 such as grasses of the genus *Brachiaria* were present (Ratter et al., 1997). Locations with signs
220 of reforestation were also avoided. Cerrado sampling sites were selected to cover the full density
221 range of this vegetation type. Five locations sampled Campo Sujo and Campo Limpo, both open
222 Cerrado types. Seven locations featured the Cerrado Sensu Stricto and five locations covered the
223 more open Campo Cerrado. Five locations featured Cerradão, the tree-dominated, closed canopy
224 Cerrado type. Five locations were sampled from both the Amazon rainforest and the Atlantic
225 rainforest. For each sampling site, five samples were collected from an area of up to 15x15
226 meters. In Cerrado areas, sampling was conducted in locations both close and distal from trees.

227 This strategy was applied because previous studies on savanna vegetation in Africa and Australia
228 found that the bulk $\delta^{13}\text{C}$ isotope composition of soils varied depending on their proximity to trees
229 (Bird et al., 2004; Wynn, 2007). Soil samples from the Llanos Basin were collected in February
230 2019. The sample set consists of transects starting in riverine back swamps and connecting
231 riparian forest vegetation with savanna vegetation. Soil samples from Caatinga shrubland
232 vegetation samples were taken in March 2020 and followed the same sampling protocol
233 described for Cerrado vegetation. In addition, we also analyzed soil and litter samples from 6
234 isolated sites from the interior of the Amazon rainforest and 2 isolated sites from the Caatinga
235 shrublands collected between 2016 and 2019.

236

237 **2.3.Laboratory procedures**

238 **2.3.1. Bulk organic analyses**

239 Total organic carbon (TOC) concentration and carbon isotopic composition ($\delta^{13}\text{C}$ OC) were
240 analyzed at the Kentucky Stable Isotope Geochemistry Laboratory (KSI GL) at the University of
241 Kentucky using a Costech 4010 Elemental Analyzer coupled via a Conflo IV to a Thermo
242 Finnigan DELTAplus XP Isotope Ratio Mass Spectrometer (IRMS). Freeze-dried, sieved (1 mm
243 mesh size) and homogenized soil samples (~50 mg) were decarbonized with 2 mL 1 M HCl at
244 50°C for 2 hours (with agitation every 30 minutes). This step was repeated as needed. Samples
245 were then rinsed with deionized water (three times or until pH reached 6-7), centrifuged, freeze-
246 dried and reweighed to assess carbonate loss. Leaf litter samples were freeze-dried and
247 powdered. Samples were weighed into pre-cleaned Sn capsules with 1-3 mg of WO_3 to promote
248 combustion. TOC concentrations were determined relative to the known TOC concentrations of
249 USGS64 (TOC = 32 %) and accounted for carbonate loss where applicable. All carbon isotope
250 values were normalized to the Vienna Pee Dee Belemnite (VPDB) scale using two
251 internationally accepted reference materials (RMs): USGS64 glycine ($\delta^{13}\text{C} = -40.81\text{‰}$) and
252 USGS41 L-glutamic acid (+37.63‰). In each analytical session, precision and accuracy were
253 assessed with multiple blind analyses of a matrix-matched RM (NIST 8704 Buffalo River
254 Sediment; $\delta^{13}\text{C} = -19.86\text{‰}$ per inter-lab comparison). The accuracy of the NIST 8704 standard
255 was 0.1% for TOC analyses and 0.1‰ for $\delta^{13}\text{C}$ analyses. The precision was 0.1% for TOC
256 analyses and 0.2‰ for $\delta^{13}\text{C}$ analyses. Sample reproducibility averaged 0.21 % (TOC) and 0.26
257 ‰ ($\delta^{13}\text{C}$).

258

259 **2.3.2. Lipid extraction and separation**

260 For lipid analysis, at the University of Southern California, samples were extracted using a
 261 Dionex Instruments ASE350 accelerated solvent extractor for two cycles of 15 minutes at 100 °C
 262 and 1500 psi using dichloromethane (DCM): methanol (MeOH) 9: 1 as solvent. Total lipid
 263 extracts (TLE) were dried under a stream of N₂. TLEs were separated into neutral and acid
 264 fractions over LC-NH₂ gel columns by subsequent elution in DCM: isopropanol 2: 1 and ethyl
 265 ether: formic acid 25: 1. The neutral fraction was further separated into apolar and polar fractions
 266 using silica gel columns and hexane and MeOH and DCM as subsequent solvents. The apolar
 267 fraction containing the *n*-alkanes was further cleaned over AgNO₃ coated silica gel columns
 268 using hexane as solvent to remove unsaturated compounds. The acid fraction was methylated at
 269 70 °C for 12 hours using MeOH: HCL 95: 5. The isotope composition of MeOH was -36.8 ± 0.2
 270 ‰ vs. VPDB. The methylated fatty acid methyl esters (FAMES) were liquid-liquid extracted
 271 using MiliQ water and hexane and transferred over Na₂SO₄ columns to remove residual water.
 272 Dried FAME fractions were then cleaned over silica gel columns using DCM as solvent. As an
 273 additional cleaning step, FAME fractions were cleaned over AgNO₃ coated silica gel columns
 274 using hexane and DCM as subsequent solvents.

275

276 **2.3.3. Lipid quantification**

277 FAMES and *n*-alkanes were quantified using an Agilent 6890 gas chromatograph coupled with a
 278 mass spectrometer (Agilent 5973) and flame ionization detector (GC-MS/FID). Compounds
 279 were identified by comparison to an external standard solution as well as their mass spectra.
 280 Quantification was achieved by comparison of the integrated peak areas to external standard
 281 solutions of known composition and concentration. The average chain length (ACL_{Alk} and
 282 ACL_{FAME}) and the carbon preference index (CPI_{Alk} and CPI_{FAME}), that is a measure of the odd vs.
 283 even chain length distribution (Cranwell, 1981), are calculated for this study as follows:

284

285

$$ACL_{Alk27-33} = \frac{27 * n-C_{27} + 29 * n-C_{29} + 31 * n-C_{31} + 33 * n-C_{33}}{n-C_{27} + n-C_{29} + n-C_{31} + n-C_{33}} \quad (1)$$

286

$$ACL_{Alk29-33} = \frac{29 * n-C_{29} + 31 * n-C_{31} + 33 * n-C_{33}}{n-C_{27} + n-C_{29} + n-C_{31} + n-C_{33}} \quad (2)$$

287

$$ACL_{FAME26-32} = \frac{26 * n-C_{26} + 28 * n-C_{28} + 30 * n-C_{30} + 32 * n-C_{32}}{n-C_{26} + n-C_{28} + n-C_{30} + n-C_{32}} \quad (3)$$

288

$$ACL_{FAME24-30} = \frac{24 * n-C_{24} + 26 * n-C_{26} + 28 * n-C_{28} + 30 * n-C_{30}}{n-C_{24} + n-C_{26} + n-C_{28} + n-C_{30}} \quad (4)$$

289

$$CPI_{Alk} = 0.5 \times \left(\frac{n-C_{27} + n-C_{29} + n-C_{31} + n-C_{33}}{n-C_{26} + n-C_{28} + n-C_{30} + n-C_{32}} + \frac{n-C_{27} + n-C_{29} + n-C_{31} + n-C_{33}}{n-C_{28} + n-C_{30} + n-C_{32} + n-C_{34}} \right) \quad (5)$$

290

$$CPI_{FAME} = 0.5 \times \left(\frac{n-C_{26} + n-C_{28} + n-C_{30} + n-C_{32}}{n-C_{25} + n-C_{27} + n-C_{29} + n-C_{31}} + \frac{n-C_{26} + n-C_{28} + n-C_{30} + n-C_{32}}{n-C_{27} + n-C_{29} + n-C_{31} + n-C_{33}} \right) \quad (6)$$

291

292 While long-chain *n*-alkanes with a chain-length between 27 and 35 carbon atoms are mostly
 293 sourced by land plants, alkanes of a shorter chain-length are mostly sourced by microbes. Hence,
 294 the ratio of mid- to long-chain *n*-alkanes ($R_{m/l}$) can be used to analyze the relative input of
 295 microbial and plant derived compounds

296

$$R_{m/l \text{ Alk}} = \frac{\sum_{i=21}^{25} n-C_i}{\sum_{i=26}^{35} n-C_i} \quad (7)$$

297

298 Likewise, we assessed the ratio of mid- to long-chain FAMES.

$$R_{m/l \text{ FAME}} = \frac{\sum_{i=14}^{23} n-C_i}{\sum_{i=24}^{34} n-C_i} \quad (8)$$

299 2.3.4. Compound-specific carbon isotope analysis

300 Compound-specific stable $\delta^{13}\text{C}$ compositions of long-chain *n*-alkanes and long-chain fatty acids
 301 were analyzed by gas chromatography–isotope ratio mass spectrometry (GC-IRMS) using a
 302 Thermo Scientific Trace gas chromatograph connected to a Delta V Plus mass spectrometer via
 303 an Isolink combustion furnace operated at 1000 °C. $\delta^{13}\text{C}$ values were determined by comparison
 304 to a reference gas and normalized to the Vienna Pee Dee Belemnite (VPDB) standard by

305 comparison to an external *n*-alkane standard containing the C₁₆ to C₃₀ *n*-alkanes and an isotope
 306 range between -28.6 and -33.3 ‰ (A3-mix by Arndt Schimmelmann, Indiana University).
 307 Measurement uncertainty was determined by calculating the root mean square error (RMSE) of
 308 the relationship between known and measured standard values used for normalization. RMSE
 309 was 0.19 ± 0.07 ‰ vs. VPDB through the measurement period. Linearity of CO₂ reference gas
 310 was checked daily across a 1 to 9 V amplitude range. The isotope composition of FAMES was
 311 corrected for the methyl group added during methylation. The majority of the samples were
 312 analyzed in duplicate.

313

314 **2.3.5. Statistical analysis**

315 Statistical analyses reported in this manuscript were performed with the statistical software R
 316 (R_Core_Team, 2022). The violin plots shown throughout the manuscript were created using the
 317 R-package ‘vioplot’ (Adler & Kelly, 2019). Tests performed included Shapiro-Wilk-tests to test
 318 for normalcy of the data, and unpaired two-sample Wilcoxon tests to test the significance of
 319 differences between vegetation types and between soil and litter samples. The test was selected
 320 since Shapiro-Wilk-tests indicated that some of the compared sample sets did not follow a
 321 normal distribution. For the same reason we also report uncertainties as interquartile ranges. For
 322 the tests between litter and soil samples, the comparison of multiple vegetation types and
 323 parameters in our sample set lead to a multiple comparisons problem, where significant
 324 differences (i.e., with a significance level of $\alpha < 0.05$) would be expected to arise by chance. To
 325 account for this issue, we used the Bonferroni correction, which is a conservative measure to
 326 correct significance levels for multiple comparisons:

$$\alpha_{\text{corrected}} = \frac{\alpha_{\text{original}}}{n} \quad (9)$$

327 Where $\alpha_{\text{corrected}}$ is the corrected significance level, α_{original} the original significance level and n the
 328 number of comparisons made.

329

330 **2.3.6. Correction for the Suess-effect**

331 To facilitate the use of our modern calibration data set for paleo vegetation reconstructions we
 332 report isotope values after correction for the Suess-effect to yield pre-industrial equivalents. In
 333 pre-industrial times (before 1750), the long-term average atmospheric $\delta^{13}\text{C}$ was around -6.5‰

334 vs. VPDB, which shifted to -8.5‰ vs. VPDB in 2019, when most of the samples were collected
 335 (Rubino et al. 2013, Keeling et al. 2005). To correct the values from litter samples we assumed
 336 recent deposition and used isotope values from the sampling year of 2019 for correction and
 337 thereby a shift of 2 ‰ since the pre-industrial:

$$338 \delta^{13}C_{corr.} = \delta^{13}C_{meas.} + \delta^{13}C_{Suess} \quad (10)$$

339
 340
 341 Where $\delta^{13}C_{corr.}$ represents the $\delta^{13}C$ composition of plant waxes corrected for the Suess-effect.
 342 $\delta^{13}C_{meas.}$ represents the analytical $\delta^{13}C$ value and $\delta^{13}C_{Suess}$ represents the shift in atmospheric
 343 $\delta^{13}C$ introduced by the Suess-effect.

344
 345 Organic matter in soils represents a mixture of different carbon ages. In tropical soils the pre-
 346 aging of topsoil organic carbon is typically minor with turnover times of around 10 years. Hence,
 347 we used the atmospheric $\delta^{13}C$ value from 2009 of -8.2‰ for correction yielding a difference of
 348 1.7‰ compared to the pre-industrial. When using *n*-alkane $\delta^{13}C$ values from the literature for
 349 comparison, we also corrected for the Suess-effect assuming an average turnover time of 10
 350 years. For samples without reported collection date, sampling in the year prior to publication was
 351 assumed.

352

353 **2.3.7. Canopy Cover**

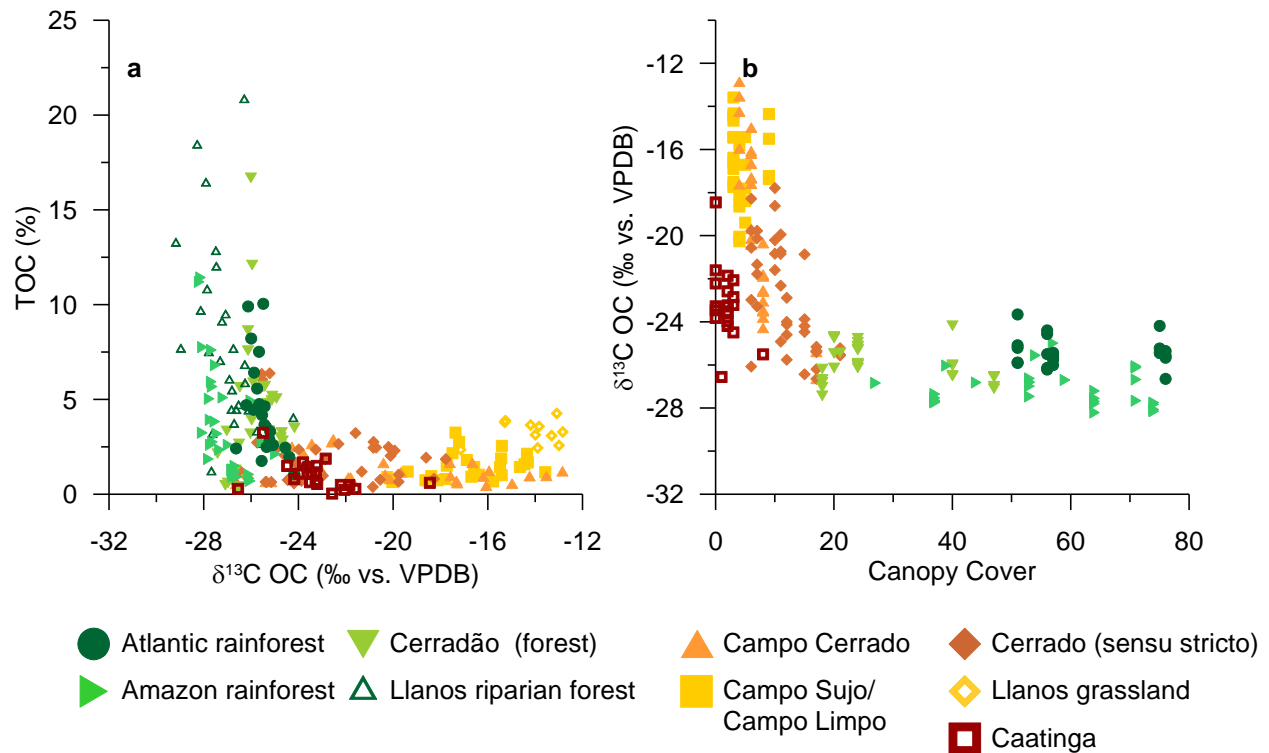
354 Tree cover data was derived from the 2015 version of the satellite derived tree cover model by
 355 Sexton et al. (2013). In the partially deforested areas of the southern Amazon, the tree cover
 356 model usually does not provide the sharp pasture/forest boundaries found in the field. Rather the
 357 transition is smoothed over several 30m × 30 meters grid cell. Locations in proximity to roads
 358 sometimes have the same effects. We adjusted the data to account for this effect by selecting
 359 values from the closest grid cell inside the forest proper and outside the artifactual transition
 360 zone in these cases.

361

362 **3. Results**

363 **3.1. Bulk organic parameters**

364 Soil TOC is highest under forest vegetation, with TOC values of up to 20% (Fig. 2a). Open
 365 savanna types and shrubland have generally lower TOC values of up to 5% (Fig. 2a). The Suess-
 366 effect corrected $\delta^{13}\text{C}$ compositions of bulk organic matter ($\delta^{13}\text{C}$ OC) in soil varies between
 367 $-29.0^{+0.6}_{-0.4}\text{‰}$ (Q_{25}^{75}) in the Amazon rainforest and $-15.5^{+0.8}_{-0.3}\text{‰}$ in Llanos savanna (Figs. 2a; S1).
 368 We thereby find the expected trend with the lowest values in multistoried rainforests and the
 369 highest values in vegetation-dominated by C_4 grasses. We find that Cerrado sensu stricto
 370 savanna has an intermediate value of $-25.3^{+1.8}_{-1.8}\text{‰}$, comparable to the mean value of $-25^{+0.8}_{-0.6}\text{‰}$
 371 in Caatinga shrubland (Fig. 2a). Forest sites have comparable $\delta^{13}\text{C}$ OC values even though
 372 canopy density varies between the dense canopies found in the Amazon and Atlantic rainforests
 373 and more open Cerradão dry forests (Fig. 2b).



374
 375 **Figure 2.** Organic parameters of surface soils from the major tropical South American vegetation
 376 types. a) Total organic carbon (TOC) vs. the stable carbon isotope composition of TOC ($\delta^{13}\text{C}$
 377 OC) corrected for the Suess-effect. b) Canopy cover inferred from Sexton et al. (2013) vs. $\delta^{13}\text{C}$
 378 OC. Since resolution of Sexton et al. (2013) did not allow the differentiation of closeby riparian
 379 forest and savanna sites of the Llanos transects, these samples are not plotted in b).

380

381 3.2. Plant wax distribution

382 For $ACL_{Alk27-33}$ we find consistent values in soil and litter samples for both forest and shrubland
 383 vegetation, while there are contrasting trends between soils and litter from the Cerrado
 384 vegetation types with higher $ACL_{Alk27-33}$ in litter than in soil (Fig. 3a). In the Llanos, savanna
 385 soils had higher $ACL_{Alk27-33}$ values than riparian forest (Fig. 3a). In contrast to $ACL_{Alk27-33}$,
 386 $ACL_{Alk29-33}$ shows a consistent trend towards higher values in both Cerrado soil and litter
 387 samples (Fig. 3c). For the $R_{m/l Alk}$, there are higher values for soil samples than in litter samples
 388 for all studied vegetation types (Figs. 3e, 6b). This discrepancy is again especially pronounced in
 389 the open Cerrado vegetation types. CPI_{Alk} values show lower values in savanna soils compared
 390 to the values observed for forests (e.g., in the Amazon rainforest $5.92^{+1.23}_{-0.37}$ and in the Campo
 391 Sujo and Campo Limpo sites $4.81^{+0.50}_{-0.73}$) (Fig. 3g). There is no consistent trend for CPI_{Alk}
 392 between litter and soil samples (Figs. 3g, 6c).

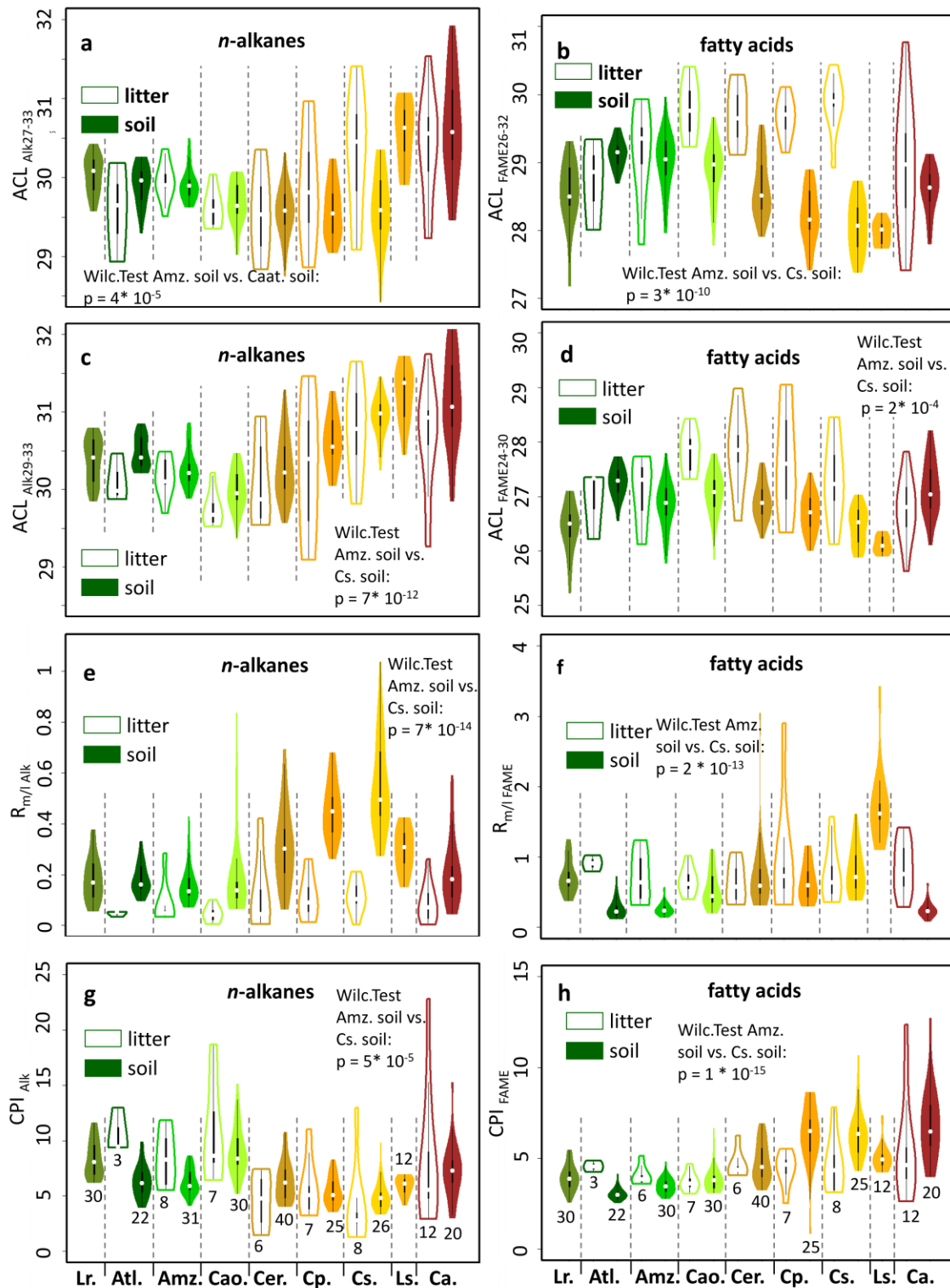
393 $ACL_{FAME26-32}$ and $ACL_{FAME24-30}$ values also show an increasing discrepancy between soil and
 394 litter samples for open Cerrado vegetation types with lower values for soil samples ($ACL_{FAME26-}$
 395 32 : $29.9^{+0.12}_{-0.08}$ in Campo Sujo/Campo Limpo litter vs. $28.07^{+0.26}_{-0.31}$ in soils) (Fig. 3b, d). The $R_{m/l}$
 396 $FAME$ showed relatively consistent values for litter samples without a difference between open
 397 and closed vegetation types. In soil samples there is a clear trend towards higher values as the
 398 vegetation density decreases (e.g., $0.24^{+0.05}_{-0.04}$ in the Amazon compared to $0.72^{+0.30}_{-0.16}$ in the Campo
 399 Sujo/Campo Limpo; Figs. 3f, 6h). Interestingly, the soil $R_{m/l FAME}$ values for forest and shrubland
 400 soils vegetation types were lower than for the litter samples of the same vegetation type, while in
 401 the open vegetation types featured similar values in soil and litter (Fig. 6h). For CPI_{FAME} , there
 402 are no distinct trends in the values of litter samples of the different vegetation types. For soil
 403 samples, there is a trend from lower values in soils from forest vegetation types (e.g., Amazon
 404 rainforest $3.48^{+0.28}_{-0.29}$) to higher values in open vegetation types (e.g., Campo Sujo/Campo Limpo
 405 $6.35^{+0.37}_{-1.01}$) and the Caatinga shrublands ($6.48^{+1.46}_{-0.78}$; Fig. 3f).

406

407 Overall, our results show that plant wax distributions in forests are more stable between litter and
 408 soil samples, while there are greater discrepancies in open savanna vegetation types (Figs. 3, 6,
 409 S2, S3).

410

411



412

413 **Figure 3.** Relative distribution of plant wax long-chain *n*-alkanes and long-chain fatty acids in

414 soil and litter samples from the major tropical South American vegetation types. a) Average

415 chain length (ACL) of the n -C₂₇ to n -C₃₃ long-chain n -alkanes. b) ACL of the C₂₆ to C₃₂ long-
 416 chain fatty acids. c) ACL of the n -C₂₉ to n -C₃₃ long-chain n -alkanes. d) ACL of the C₂₄ to C₃₀
 417 long-chain fatty acids. e) $R_{m/l}$ Alk. f) $R_{m/l}$ FAME. g) Carbon preference index (CPI) of long-chain n -
 418 alkanes. h) CPI of long-chain fatty acids. The black lines in the violin plot represent box-whisker
 419 plots and the white point the median. The violins represent kernel density plots that are cut off at
 420 the data limits. The numbers below the violin plots indicate the number of samples represented
 421 by each plot. Abbreviations are as follows: Lr: Llanos riparian forest. Atl: Atlantic rain forest.
 422 Amz: Amazon rainforest. Cao: Cerradão dry forest. Cer: Cerrado sensu stricto. Cp: Campo
 423 Cerrado. Cs: Campo Sujo/Campo Limpo. Ls: Llanos savanna. Ca: Caatinga shrublands. From the
 424 Llanos samples, only soil material was available. For complete chain length distributions of the
 425 litter and soil samples see Figs. S2 and S3.

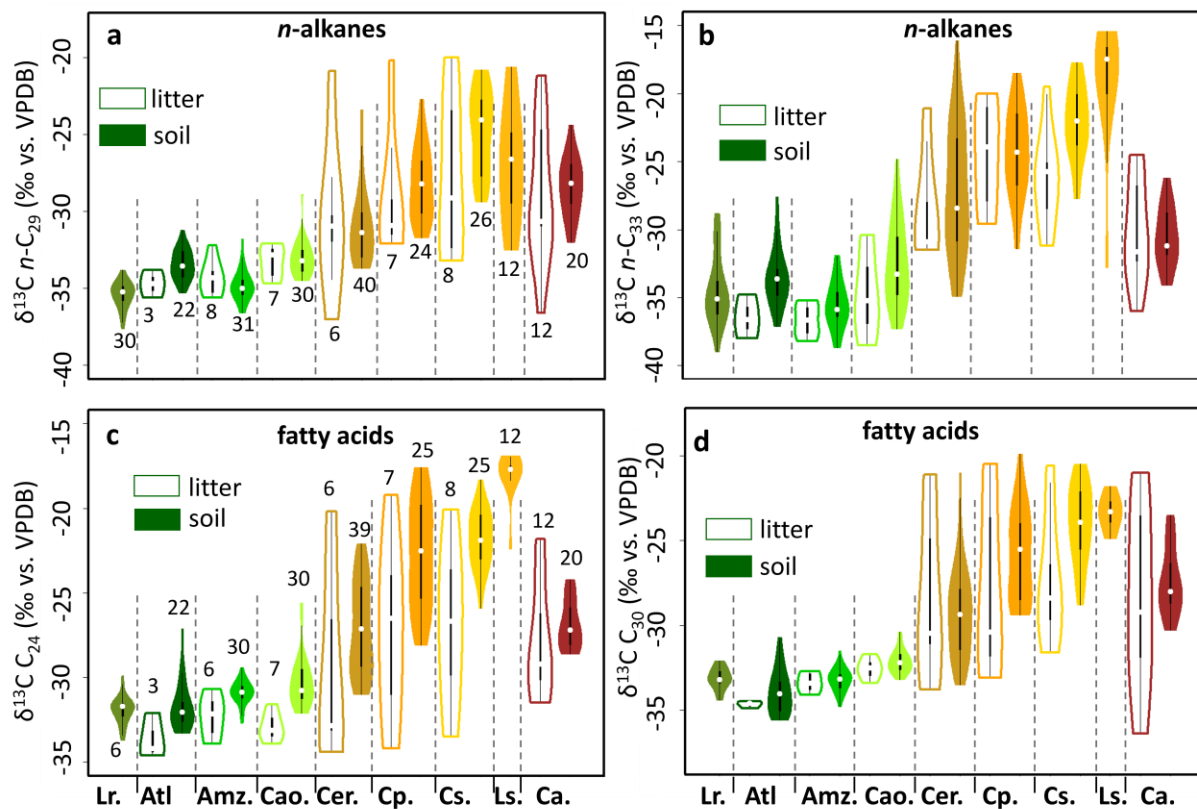
426

427 3.3.Plant wax isotope composition

428 The $\delta^{13}\text{C}$ composition of all plant wax homologues shows a pattern that is similar to the one
 429 described for $\delta^{13}\text{C}$ OC (Fig. 2), with higher values for more open vegetation types and the lowest
 430 values in the Atlantic and Amazon rainforests as well as the Llanos riparian forests (Fig. 4a-d).
 431 Litter and soil samples also showed broadly consistent patterns (Fig. 4a-d, Fig. 6d,e,j,k). Aside
 432 from the broad general trend towards higher values in open vegetation types, there are some
 433 pronounced differences among compounds and homologues, especially n -alkanes of varying
 434 chain-lengths.

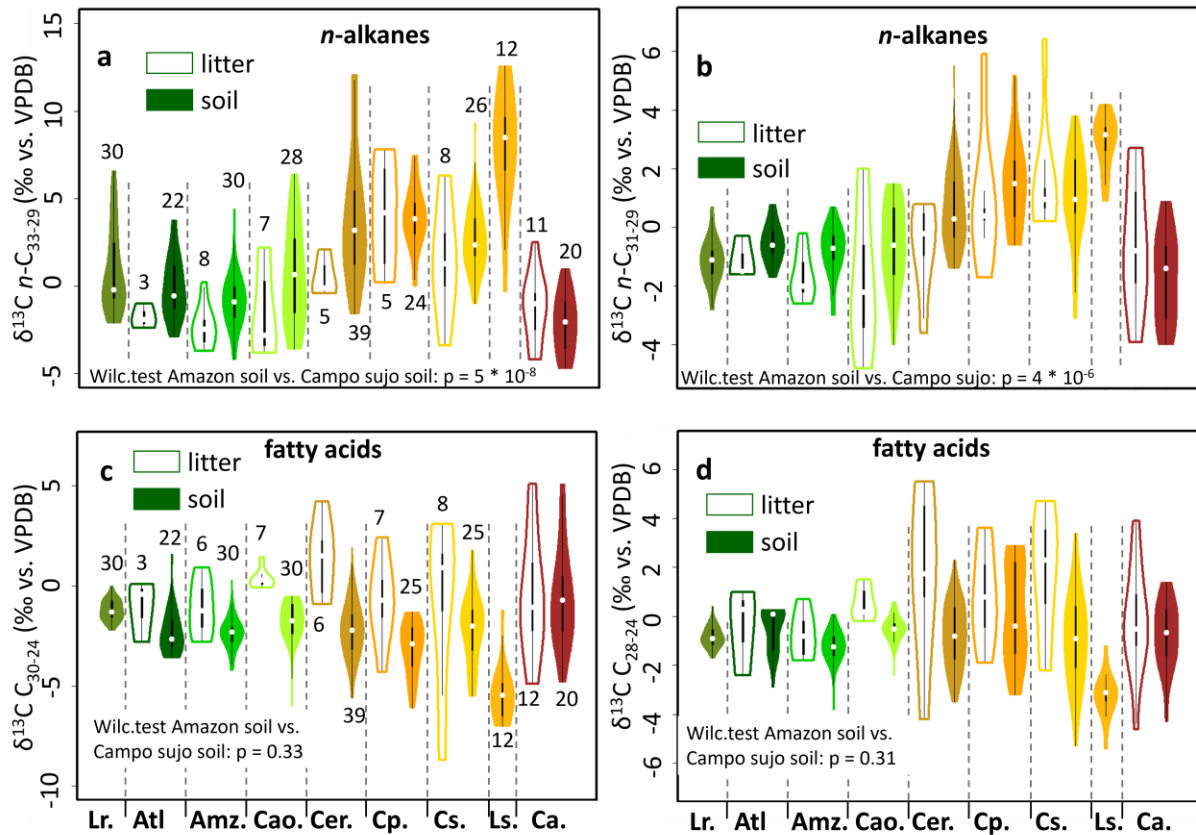
435 The $\delta^{13}\text{C}$ composition of n -C₂₉ long-chain n -alkanes ($\delta^{13}\text{C}$ C₂₉) from Cerrado sensu stricto soils
 436 shows, for instance, lower values ($-31.4 \pm_{-1.6}^{+1.3}$ ‰) than the $\delta^{13}\text{C}$ composition of the n -C₃₃ n -
 437 alkanes ($-28.4 \pm_{-2.5}^{+5.1}$ ‰) (Fig. 4a). In forest formations, both homologues have comparable values
 438 (e.g., Amazon rainforest: $\delta^{13}\text{C}$ C₂₉: $-35.0 \pm_{-0.4}^{+0.5}$ ‰; $\delta^{13}\text{C}$ C₃₃: $-35.9 \pm_{-0.5}^{+1.3}$ ‰), while in Caatinga
 439 shrublands $\delta^{13}\text{C}$ C₂₉ is even higher than $\delta^{13}\text{C}$ C₃₃ ($\delta^{13}\text{C}$ C₂₉: $-28.2 \pm_{-1.3}^{+1.2}$ ‰; $\delta^{13}\text{C}$ C₃₃: $-31.2 \pm_{-0.6}^{+2.4}$
 440 ‰) (Fig. 4a). This leads to a pattern, where the difference between $\delta^{13}\text{C}$ C₃₃ and $\delta^{13}\text{C}$ C₂₉ ($\delta^{13}\text{C}$
 441 C₃₃₋₂₉) has small or negative values in forests (e.g., Amazon rainforest $-0.9 \pm_{-0.9}^{+0.9}$ ‰; Fig. 5a) and
 442 Caatinga shrublands ($-2.1 \pm_{-1.5}^{+1.2}$ ‰), while open vegetation types have positive values (e.g.,
 443 Cerrado sensu stricto ($3.2 \pm_{-1.9}^{+2.3}$ ‰; Fig. 5a). A similar, albeit less pronounced pattern also arises
 444 for the difference between $\delta^{13}\text{C}$ C₃₁ and $\delta^{13}\text{C}$ C₂₉ ($\delta^{13}\text{C}$ C₃₁₋₂₉; Fig. 5b). Leaf litter n -alkanes show
 445 the same pattern described above (Fig. 6d, e, f).

446 The $\delta^{13}\text{C}$ composition of different long-chain fatty acids homologues (e.g., $\delta^{13}\text{C}$ C_{24} and C_{30})
 447 also shows the expected trends, with higher values in more open vegetation types (Fig. 4c, d). In
 448 contrast to long-chain *n*-alkanes, differences between different homologues ($\delta^{13}\text{C}$ C_{30} and $\delta^{13}\text{C}$
 449 C_{24} ($\delta^{13}\text{C}$ C_{30-24}), as well as between $\delta^{13}\text{C}$ C_{28} and $\delta^{13}\text{C}$ C_{24} ($\delta^{13}\text{C}$ C_{28-24}) are not significantly
 450 distinct between rainforest and open vegetation types (Figs. 5c, d). There is a consistent offset in
 451 values between the fatty acids of different homologues with higher values in homologues of
 452 shorter chain length. This leads to a pattern where C_{24} compounds in soils have $2.1^{+0.8}_{-0.9}$ ‰
 453 higher values than C_{30} homologues (Fig. 5c). On average, the $\delta^{13}\text{C}$ composition of different long-
 454 chain fatty acids in litter samples is slightly lower than in soils (Figs. 6j, k, l).



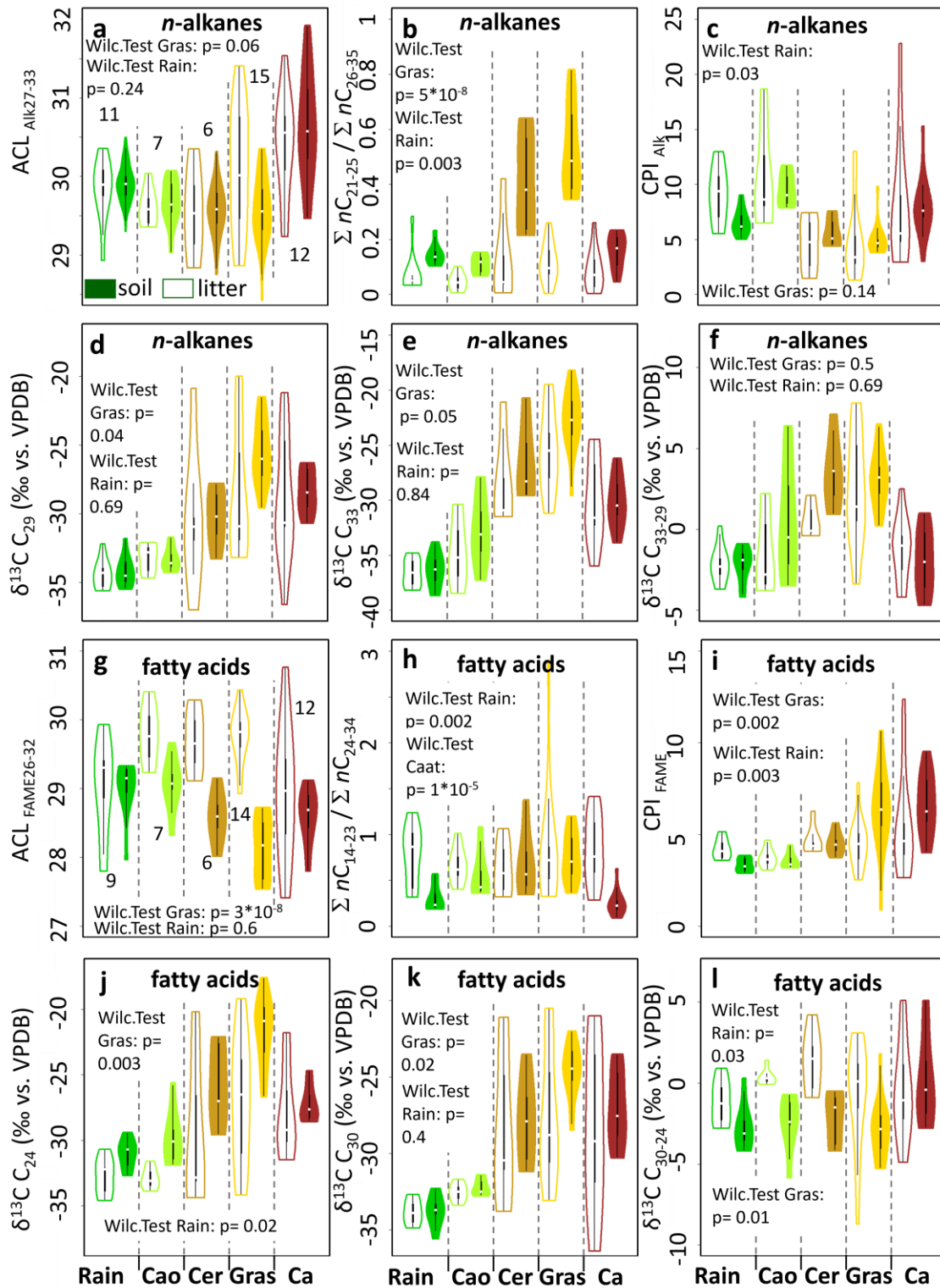
455
 456 **Figure 4.** Stable carbon isotope composition ($\delta^{13}\text{C}$) of long-chain *n*-alkanes and long-chain fatty
 457 acids in soil and litter samples from the major tropical South American vegetation types. a) $\delta^{13}\text{C}$
 458 composition of the C_{29} long-chain *n*-alkane. b) $\delta^{13}\text{C}$ composition of the C_{33} long-chain *n*-alkane.
 459 c) $\delta^{13}\text{C}$ composition of the C_{24} long-chain fatty acid d) $\delta^{13}\text{C}$ composition of the C_{30} long-chain
 460 fatty acid. The black lines in the violin plot represent box-whisker plots and the white point the
 461 median. The violins represent kernel density plots that are cut off at the data limits. The numbers
 462 adjacent to the violin plots indicate the number of samples represented by each plot. Panels a)

463 and b) have the same sample numbers as do panels c) and d). Abbreviations are as follows: Lr:
 464 Llanos riparian forest. Atl: Atlantic rain forest. Amz: Amazon rainforest. Cao: Cerradão dry
 465 forest. Cer: Cerrado sensu stricto. Cp: Campo Cerrado. Cs: Campo Sujo. Ls: Llanos savanna. Ca:
 466 Caatinga shrublands. From the Llanos samples, only soil material was available.
 467



468
 469
 470 **Figure 5.** Variations in stable carbon isotope composition ($\delta^{13}\text{C}$) among long-chain *n*-alkane and
 471 long-chain fatty acid homologues in soil and litter samples from the major tropical South
 472 American vegetation types. a) Difference between the $\delta^{13}\text{C}$ composition of the *n*- C_{33} and *n*- C_{29}
 473 long-chain *n*-alkanes. b) Difference between the $\delta^{13}\text{C}$ composition of the *n*- C_{31} and *n*- C_{29} long-
 474 chain *n*-alkanes c) Difference between the $\delta^{13}\text{C}$ composition of the C_{30} and the C_{24} long-chain
 475 fatty acids. d) Difference between the $\delta^{13}\text{C}$ composition of the C_{28} and the C_{24} long-chain fatty
 476 acids. The black lines in the violin plot represent box-whisker plots and the white point the
 477 median. The violins represent kernel density plots that are cut off at the data limits. The numbers
 478 below or above the violin plots indicate the number of samples represented by each violin.

479 Abbreviations are as follows: Lr: Llanos riparian forest. Atl: Atlantic rain forest. Amz: Amazon
480 rainforest. Cao: Cerradão dry forest. Cer: Cerrado sensu stricto. Cp: Campo Cerrado. Cs: Campo
481 Sujo/Campo Limpo. Ls: Llanos savanna. Ca: Caatinga shrublands. From the Llanos samples,
482 only soil material was available.



483

484 **Figure 6.** Relationship between litter and soil long-chain *n*-alkanes and long-chain fatty acid

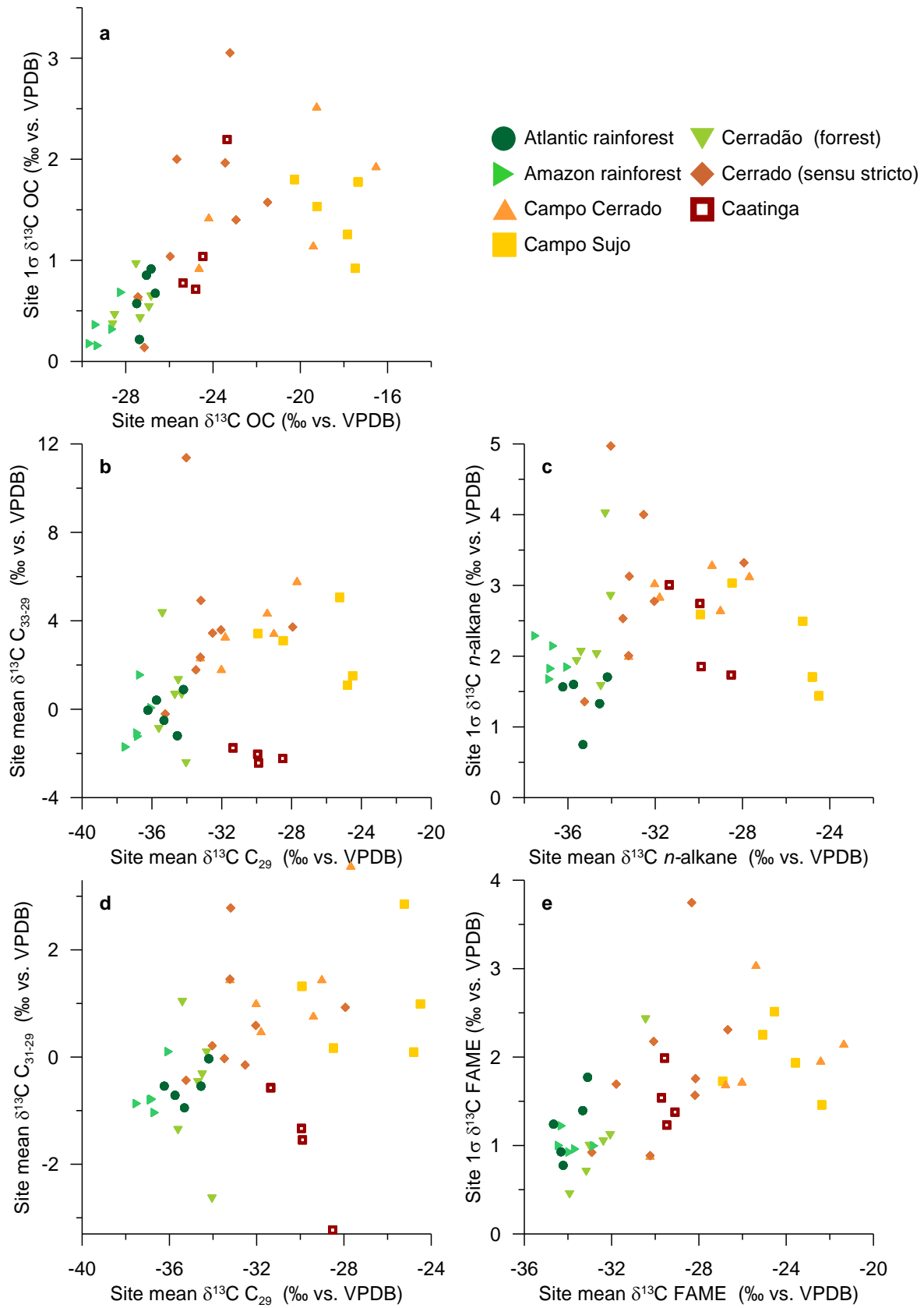
485 distributions and stable carbon isotope compositions ($\delta^{13}\text{C}$) in soil and litter samples from the

486 major tropical South American vegetation types. To allow for a direct comparison between litter
 487 and soil, the figure only features soil samples that also have corresponding litter samples. a)
 488 Average chain length ($ACL_{Alk27-33}$) of long-chain *n*-alkanes. b) $R_{m/l Alk}$. c) Carbon preference
 489 index (CPI) of long-chain *n*-alkanes. d) $\delta^{13}C$ composition of the C_{29} long-chain *n*-alkane. e) $\delta^{13}C$
 490 composition of the C_{33} long-chain *n*-alkane f) Difference between the $\delta^{13}C$ composition of the *n*-
 491 C_{29} and *n*- C_{33} long-chain *n*-alkanes. g) ACL of long-chain fatty acids ($ACL_{FAME26-32}$). h) $R_{m/l}$
 492 $FAME$. i) CPI of long-chain fatty acids. j) $\delta^{13}C$ composition of the C_{24} long-chain fatty acid. k)
 493 $\delta^{13}C$ composition of the C_{30} long-chain fatty acid. l) Difference between the $\delta^{13}C$ composition of
 494 the C_{24} and the C_{30} long-chain fatty acids. The reported Wilcoxon tests were made between litter
 495 and soil samples of the indicated vegetation types. The black lines in the violin plot represent
 496 box-whisker plots and the white point the median. The violins represent kernel density plots that
 497 are cut off at the data limits. The numbers below the violin plots indicate the number of samples
 498 represented by each plot. Abbreviations are Rain: rainforests (Amazon & Atlantic), Cao:
 499 Cerradão dry forest. Cer: Cerrado sensu stricto. Gras: Open grass-dominated Cerrado
 500 physiognomies (Campo Sujo/Campo Limpo and Campo Cerrado). Ca: Caatinga shrublands. Due
 501 to the multiple comparisons conducted for each proxy, the corrected significance level using the
 502 Bonferroni correction would be 0.01, since 5 comparisons were conducted for each panel.

503

504 **3.4. Local variability**

505 The variability of $\delta^{13}C$ values among the five samples taken at each site shows matching trends
 506 for $\delta^{13}C$ OC and plant waxes (Fig. 7a, c, e). For the forests, we observe relatively stable values,
 507 while there is an increase in variability in the Cerradão dry forest and Caatinga shrubland sites
 508 (Fig. 7a, c, e). Variability is maximal for the mixed Cerrado sensu stricto and Campo Cerrado
 509 sites and slightly lower again for the Campo Sujo/Campo Limpo sites (Fig. 7a, c, e). With the
 510 exception of Caatinga shrublands, this pattern is similar to the trends observed for $\delta^{13}C$ C_{33-29} and
 511 $\delta^{13}C$ C_{31-29} (Fig. 7b, d).



512

513 **Figure 7.** Site specific variation in the stable carbon isotope composition ($\delta^{13}\text{C}$) of plant wax *n*-
 514 alkanes ($\delta^{13}\text{C}$ *n*-alkane), fatty acids ($\delta^{13}\text{C}$ fatty acid) and bulk organic carbon ($\delta^{13}\text{C}$ OC). a)
 515 Standard deviation ($1\ \sigma$) of all $\delta^{13}\text{C}$ OC values at each site. b) Site average of $\delta^{13}\text{C}$ C_{33-29} . c)
 516 Standard deviation of the $\delta^{13}\text{C}$ values among all long-chain *n*-alkane (*n*- $\text{C}_{27,29,31,33}$) homologues
 517 at each site. d) Site average of $\delta^{13}\text{C}$ C_{31-29} . e) Standard deviation of the $\delta^{13}\text{C}$ values of all long-
 518 chain fatty acid ($\text{C}_{24,26,28,30}$) homologues at each site.

519

520 **4. Discussion**

521 **4.1. Bulk organic parameters**

522 The highest TOC contents in surface soil samples from tropical South America are found under
 523 forests, while savanna and shrubland samples yielded on average lower TOC (Fig. 2a). This
 524 finding is in line with global trends found in previous studies (Minasny et al., 2017; Stockmann
 525 et al., 2015). The $\delta^{13}\text{C}$ composition of soil organic carbon also shows expected patterns with the
 526 highest values in open savannas that hold the highest proportion of C_4 grass species (Campo Sujo
 527 and Campo Limpo) and the lowest values in tropical rainforests (Amazon rainforest; Fig. 2a).
 528 Cerrado sensu stricto show similar values to the semi-arid Caatinga shrublands, both being
 529 intermediate between forests and the most open savannas. The carbon isotope values measured in
 530 Caatinga soil samples are consistent with an extensive data set of $\delta^{13}\text{C}$ OC from leaves of
 531 Caatinga shrubs (Martinelli et al., 2020). In contrast to savannas, where $\delta^{13}\text{C}$ values are
 532 controlled by the relative input of C_3 and C_4 species, $\delta^{13}\text{C}$ values in Caatinga shrublands are also
 533 increased by the aridity effects on C_3 plants caused by drier conditions with MAP values around
 534 $500\ \text{mm}\ \text{y}^{-1}$ found in northeastern Brazil (Karger et al., 2017; Martinelli et al., 2020). Under arid
 535 conditions, a decrease in leaf stomatal conductance is thought to lead to a decrease of the
 536 intercellular pCO_2 resulting in a decrease in fractionation during carbon fixation (Diefendorf et
 537 al., 2010; Kohn, 2010). In addition, CAM plants such as cacti and other succulents are abundant
 538 in Caatinga vegetation. While CAM plants can feature a wide range of $\delta^{13}\text{C}$ OC values, they tend
 539 to be intermediate between C_3 and C_4 plants (Messerschmid et al., 2021) and thereby also
 540 contribute to the observed $\delta^{13}\text{C}$ OC in the Caatinga $\delta^{13}\text{C}$ data set. The values observed for
 541 Caatinga thereby reflect the combination of aridity and photosynthesis effects.

542

543 **4.2. Relative distribution of plant waxes**

544 4.2.1. Microbial overprint

545 The relative distributions of plant waxes show substantial shifts from litter to soil samples as
546 well as among different vegetation types (Figs. 3; 6a-c, g-i). The magnitude of the shifts between
547 litter and soils tends to be larger for open savannas than for rainforests and the most significant
548 shifts were observed for the $R_{m/Alk}$ and $ACL_{FAME26-32}$ of the open Cerrado vegetation types (Figs.
549 3; 6a-c, g-i).

550 Fresh angiosperm plant material typically has low amounts of mid-chain *n*-alkanes (Bush &
551 McInerney, 2013). The increase in mid-chain *n*-alkanes in soils is therefore likely caused by
552 microbial overprint and can either be the result of the addition of compounds by fresh microbial
553 synthesis (Nguyen Tu et al., 2011) or by the reworking of longer-chain compounds into shorter
554 chain homologues by microbes (Brittingham et al., 2017). While this input is minor for
555 rainforests, as previously reported from soils of the Amazon rainforest and Andean cloud forests
556 (Wu et al., 2019), the encroachment of microbial compounds is more pronounced in soils from
557 the savannas of the Cerrado and the Llanos Basin (Figs. 3c; 6b; S2a-i).

558 Shifts in the relative distribution of *n*-alkanes due to microbial overprint not only affect mid-
559 chain compounds with a carbon chain-length ≤ 25 but also affect longer chain-length
560 compounds. $ACL_{Alk27-33}$ shows lower values in soils from open Cerrado types than in soils from
561 forest vegetation (Figs. 3a, 6a). This contrasts with the trend found in litter samples as well as
562 with the findings from the Llanos savannas and other tropical savannas in Africa and Australia
563 (Figs. 3a, 6a) (Krull et al., 2006; Rommerskirchen et al., 2006). For $ACL_{Alk29-33}$, which does not
564 take the C_{27} *n*-alkane into account, soils from open Cerrado types show the expected trends
565 towards higher values (Fig. 3c). This indicates that microbial overprint in Cerrado savanna
566 samples can also lead to an increase in the relative contribution of the C_{27} *n*-alkane, while the
567 relative distribution of the longer-chain *n*-alkanes remains relatively stable during incorporation
568 into soils. Further evidence for the stability of the distribution of longer-chain compounds is also
569 provided by the consistent CPI values between litter and soil samples of all studied vegetation
570 types (Figs. 3g, 6c).

571 $ACL_{FAME26-32}$ and $ACL_{FAME24-30}$ from savannas vegetation types are also affected by microbial
572 overprint and feature lower values in soils than in litter (Figs. 3b, d; 6g). This can be caused by
573 the reworking to compounds of shorter chain-length, the fresh synthesis of shorter-chain
574 homologues, or by the conversion of *n*-alkanes to fatty acids (Ji et al., 2013; Ofiti et al., 2021). In

575 contrast to *n*-alkanes, fatty acids with shorter chain-length between 16 and 23 carbon atoms can
576 also be dominant in angiosperm leaf material (Almendros et al., 1996; Chikaraishi & Naraoka,
577 2006), leading to a more complex picture than for long-chain *n*-alkanes (Figs. 3d, 6h). Since
578 shorter-chain length compounds are already present in leaves, microbial turnover during
579 incorporation into soils can both lead to a lowering in $R_{m/l \text{ FAME}}$ resulting from the preferential
580 degradation of shorter-chain fatty acids and to an increase in $R_{m/l \text{ FAME}}$ due to the fresh
581 synthesis of shorter chain-length compounds (Chikaraishi & Naraoka, 2006). The lowering of
582 $R_{m/l \text{ FAME}}$ values in soils from forests and Caatinga shrubland therefore suggest that degradation
583 is the dominant process there (Figs. 3d, 6g,h). For the other vegetation types the two processes
584 seem to be balanced, leading to comparably stable relative contributions of mid-chain
585 compounds (Figs. 3d, 6h). Another interesting aspect of the consequences of microbial overprint
586 can be observed in CPI_{FAME} . While CPI_{FAME} of forests shows the expected trend towards lower
587 values in soils compared to litter, there is a trend towards higher values for CPI_{FAME} in soils of
588 open vegetation types (Fig. 6i). When the relative individual contributions of long-chain fatty
589 acids are considered, it becomes apparent that the odd-chain compounds from savannas show
590 similar contributions for both litter and soil samples (Fig. S3). Rather than a decrease in the
591 relative contribution of odd-chain length compounds, the main cause for the increased CPI_{FAME}
592 values is an enhanced contribution of C_{24} , C_{26} and C_{28} fatty acids (Fig. S3). Soils from open
593 Cerrado vegetation types also show a decrease in C_{32} and C_{34} between soil and litter, which is
594 however not part of the formulation of CPI_{FAME} . Hence, the increase in CPI_{FAME} in soils from
595 savannas is likely the effect of the overall shift towards shorter even-chained homologues (Fig.
596 S3).

597 Overall, our results consistently show a more pronounced microbial overprint in savannas than in
598 forests. Multiple mechanisms may lead to this pattern. First, grasses produce generally lower
599 amounts of long-chain *n*-alkanes compared to tropical trees leaving savannas more prone to
600 microbial overprint. Second, the studied savannas have soils with relatively low pH values of
601 $5^{+0.3}_{-0.3}$. In acidic soils, *n*-alkanes have been reported to be less well preserved than fatty acids
602 (Bull et al., 2000; Wu et al., 2019), which potentially further reduced *n*-alkane concentrations
603 facilitating overprint. In addition, microbes using alkane hydroxylase can also convert long-chain
604 *n*-alkanes to long-chain fatty acids (Ji et al., 2013), which may have contributed to the relative
605 increase in C_{24} , C_{26} and C_{28} fatty acids in savanna soils (Fig. S3). Again, such mechanism would

606 lead to more pronounced effects in savanna vegetation, that synthesize smaller amounts of plant
607 waxes. Another factor that might additionally lead to the lower average chainlength of fatty acid
608 and *n*-alkanes is the high fire activity in the Cerrado savanna (Pivello, 2011), since soils from fire
609 affected areas typically yield long-chain *n*-alkane and fatty acid compounds with lower chain
610 length (Eckmeier & Wiesenberg, 2009; Faria et al., 2015).

611
612 Our finding of increased mid-chain *n*-alkane contributions in savanna soils relative to the
613 respective litter samples is corroborated by concentrations of mid-to-long chain compounds in
614 the Serengeti savanna soils in Africa (Zhang et al., 2021). Microbial production of mid-chains in
615 savanna soils has implications for the use of the ratio of mid-to-long chain *n*-alkanes as proxy for
616 aquatic OC contributions in lacustrine sediments (Ficken et al., 2000). As savanna soils carry
617 $R_{m/1\text{ Alk}}$ values similar to those found in lakes with heavy aquatic contributions, this ambiguity
618 has to be considered when interpreting alkane distributions in savanna-bordered aquatic settings.
619 Overprint also complicates interpretation of $ACL_{\text{Alk}27-33}$, which has been proposed as an indicator
620 of climate and vegetation change (Bush & McInerney, 2015; Chen et al., 2022; Rommerskirchen
621 et al., 2006). We therefore recommend using $ACL_{\text{Alk}29-33}$ to avoid the effects of microbial
622 overprint.

623

624 **4.2.2. Relation to vegetation and climate**

625 Microbial overprint has no significant effect on the relative distribution of long-chain *n*-alkanes
626 with a chain-length ≥ 29 . For these compounds, the $ACL_{\text{Alk}29-33}$ shows higher values in more
627 open savannas and in Caatinga compared to forests (Fig. 3c). The trend towards higher values in
628 tropical savannas has been previously observed in Africa and Australia (Krull et al., 2006; J. Liu
629 et al., 2022; Rommerskirchen et al., 2003; Rommerskirchen et al., 2006). Likewise, the higher
630 values for xeric shrublands have also been observed in African shrublands (Carr et al., 2014).
631 $ACL_{\text{Alk}29-33}$ from open Cerrado vegetation types show a larger variability in litter samples than
632 the ones from soils, demonstrating the wide variability that *n*-alkane distributions can have on a
633 species level, as well as the integrating nature of soils (Fig. 3c). For Caatinga shrublands, we also
634 find a large range of $ACL_{\text{Alk}29-33}$ in both litter and soils. This is in line with findings from shrubs
635 and succulents from xeric shrublands in Africa that feature a wide range of different *n*-alkane
636 distributions (Boom et al., 2014; Carr et al., 2014; Feakins & Sessions, 2010). Given that xeric

637 shrublands are often sparsely vegetated, the large differences introduced by individual plants
638 may be locally preserved in Caatinga soils, whereas greater averaging is expected in Cerrado
639 savanna soils.

640 On a biome-integrated scale, the *n*-alkane patterns in tropical South American and African
641 savannas and shrublands show remarkable consistency despite the different evolutionary origin
642 of the savannas on these continents (Edwards et al., 2010). This may be the result of convergent
643 adaptation of leaf-wax *n*-alkane traits of the dominant grass and shrubland species to
644 environmental factors (C.-K. Yang et al., 2018), or represent traits deeply rooted in plant
645 phylogeny. Given that there are additional factors such as altitude and climate variables that
646 affect *n*-alkane distributions (Bush & McInerney, 2015; Feakins et al., 2016) we emphasize that
647 the chemotaxonomic significance of our sampling is limited to the study region. In contrast to
648 previous regional studies (Bush & McInerney, 2015), we do not observe an impact of climatic
649 variables on long-chain *n*-alkane distributions. For example, we find that xeric shrubland (MAP
650 $\sim 500 \text{ mm y}^{-1}$) has similar $\text{ACL}_{\text{Alk29-33}}$ values to Llanos savanna with $\text{MAP} > 2000 \text{ mm y}^{-1}$ (Fig.
651 3c). The absence of a relation to climate variables here is unsurprising, since the various
652 relationships observed in regional studies, even though they may be statistically significant
653 (Chen et al., 2022) have proven too weak and variable to be generalizable for
654 paleoenvironmental research on a global level.

655

656 **4.3.Plant wax isotope compositions as proxies for vegetation in tropical South America**

657 **4.3.1. Stability during incorporation into soil**

658 The leaf litter and soil plant wax $\delta^{13}\text{C}$ data follows the expected trend with higher $\delta^{13}\text{C}$ values in
659 more open vegetation (Fig. 4). Similar to the pattern observed for the relative distribution of
660 long-chain *n*-alkanes and long-chain fatty acids, we also find that the variability of isotope values
661 in leaf litter is greater than in the underlying soils. Again, the variability is especially pronounced
662 for the savanna and shrubland vegetation types (Figs. 4, 5, 6d-f; j-l). For forests, the plant wax
663 isotope data of long-chain *n*-alkanes and long-chain fatty acids is consistent among leaf litter and
664 soil samples (Fig. 6d-f). For savannas, the large variability found in litter complicates the
665 assessment of the effect of incorporation into soils; although Cerrado litter samples have on
666 average lower values than soils, the difference is not significant due to the large variability found
667 in both populations (Fig. 6d, e, j, k). While there is considerable variability for separate

668 homologues, the consistency in $\delta^{13}\text{C}$ C_{33-29} values between soil and litter suggests that the isotope
 669 values in savanna and shrubland areas are relatively stable during soil incorporation as well (Fig.
 670 6f). The consistency in isotope values found for the forest samples somewhat contrast previous
 671 work that found shifts in $\delta^{13}\text{C}$ compositions during incorporation of plant waxes into soils
 672 (Chikaraishi & Naraoka, 2006; Tu et al., 2004; Wu et al., 2019; Y. Zhang et al., 2017). Evidence
 673 from litter bag experiments studying the evolution of plant wax $\delta^{13}\text{C}$ compositions during
 674 degradation also paint an inconsistent picture, with some reporting effects on the isotope
 675 composition, while others do not (Huang et al., 1997; Nguyen Tu et al., 2011). This indicates that
 676 the impact of degradation on plant wax $\delta^{13}\text{C}$ might have varying outcomes under different
 677 conditions. These might include varying vegetation types with as well as different climate
 678 conditions or fire activity (Sarangi et al., 2022). We also note that our study focused on the upper
 679 5 cm of the sampled soils, and deeper soil horizons might feature the enrichment observed
 680 elsewhere.

681

682 **4.3.2. Differentiating South American vegetation types using plant wax isotopes**

683 While C_3 plants can cover a wide range of isotope compositions our dataset shows that both the
 684 litter and soil samples from the different forest types of the studied area cover a relatively narrow
 685 range of values (Fig. 4 a-d). For instance, the Suess-effect corrected $\delta^{13}\text{C}$ C_{29} of the combined
 686 Atlantic and Amazon rainforests, the Cerradão dry forest and Llanos riparian forests a show a
 687 range of $-34.4 \pm_{0.7}^{+1.1}$ ‰ (Fig. 4a). Values above that range can indicate savanna or shrubland
 688 intrusions, even though there are C_3 species that might have higher $\delta^{13}\text{C}$. Indeed, the interquartile
 689 range of $\delta^{13}\text{C}$ C_{29} values found in soils from our Cerrado sensu stricto sample set (i.e.,
 690 $-31.4 \pm_{1.6}^{+1.3}$; Fig. 4a) is well within the range covered by some C_3 plants (J. Liu & An, 2020).
 691 Although $\delta^{13}\text{C}$ C_{29} values in Cerrado sensu stricto can still be in the range of forest samples, $\delta^{13}\text{C}$
 692 C_{33} values are more sensitive to contributions by grass vegetation. The cause for this difference
 693 lays in the different production of homologues by grass and tree taxa. Tree-dominated vegetation
 694 types have long-chain *n*-alkane distributions dominated by *n*- C_{29} and *n*- C_{31} homologues with low
 695 proportions of *n*- C_{33} (Figs. S2). In contrast, grass-dominated vegetation types have more uniform
 696 homologue distribution and comparable contributions of *n*- C_{29} , *n*- C_{31} and *n*- C_{33} (Fig. S2).
 697 Therefore, the addition of grasses with a higher C_{33} homologue contributions leads to a more
 698 pronounced impact on $\delta^{13}\text{C}$ C_{33} values than on $\delta^{13}\text{C}$ C_{29} values (Figs. 4b, S4). Indeed, the

699 Cerradão dry forests, which can be in transition into Cerrado sensu stricto, feature the overall
700 highest relative contribution of n -C₂₉, leading to a strong impact of n -C₃₃ provided by minor
701 grass contributions (Fig. S2). Likewise, the addition of tree derived n -alkanes to a grass-
702 dominated environment leads to a more pronounced response in $\delta^{13}\text{C}$ C₂₉ than in $\delta^{13}\text{C}$ C₃₃ (Fig.
703 4a, b). Our observation that $\delta^{13}\text{C}$ of different long-chain n -alkane homologues show a nuanced
704 response to shifts in vegetation has also been made in savanna areas from Africa, D. (Garcin et
705 al., 2014; Schwab et al., 2015; D. Zhang et al., 2021). While the $\delta^{13}\text{C}$ of different long-chain n -
706 alkane homologues yield distinct sensitivity to tree or grass input, the $\delta^{13}\text{C}$ of long-chain fatty
707 acids show more consistent trends among different homologues (Fig. 4c, d). Fatty acid $\delta^{13}\text{C}$
708 compositions are also more similar to $\delta^{13}\text{C}$ OC than long-chain n -alkanes (Figs. S4, S5). Since
709 fatty acids have more homogeneous chain-length distributions among different vegetation types,
710 the mixing between tree and grass genera does not lead to shifts that are focused on specific
711 homologues but rather affect all reported compounds.

712 Our data shows that the $\delta^{13}\text{C}$ composition of both long-chain n -alkanes and long-chain fatty
713 acids from Cerrado sensu stricto is similar to semi-arid Caatinga shrublands (Fig. 4a-d). Hence,
714 the $\delta^{13}\text{C}$ of single plant wax homologues or pooled data of multiple homologues cannot be used
715 to differentiate between shrubland and savanna vegetation types found under distinctly different
716 climate conditions, complicating interpretations of plant-wax records (Boom et al., 2014). As
717 discussed for soil $\delta^{13}\text{C}$ OC, the enrichment in Caatinga vegetation is partly the result of drier
718 conditions and CAM photosynthesis (da Silva & Lacher, 2020; J. Liu & An, 2020; Martinelli et
719 al., 2020). Our results therefore indicate that the interpretation of plant wax $\delta^{13}\text{C}$ compositions as
720 recorders of relative contributions of C₃ and C₄ plants on a forest-savanna continuum is
721 incomplete, as shrublands may produce similar values to savannas (Goñi et al., 1997; Huang et
722 al., 2000; Schefuß et al., 2005). As xeric shrublands cover substantial tropical areas (Olson et al.,
723 2001), this has major implications for the interpretation of the $\delta^{13}\text{C}$ of plant waxes as
724 paleoenvironmental proxies and calibration studies treating $\delta^{13}\text{C}$ values in sedimentary archives
725 as binary mixtures between C₃ and C₄ endmembers (Magill et al., 2013; D. Yang & Bowen,
726 2022).

727

728 **4.4. Multi-homologue isotope assessment of tropical vegetation structure**

729 **4.4.1. Tropical South America**

730 While single homologue or bulk organic matter analysis cannot differentiate between Cerrado
731 sensu stricto and semi-arid Caatinga shrublands, our data show substantial differences between
732 the two vegetation types for $\delta^{13}\text{C}$ C₃₃₋₂₉ or $\delta^{13}\text{C}$ C₃₁₋₂₉ (Fig. 5, a, b). Here, samples from Cerrado
733 savanna have substantially higher values than from Caatinga shrubland samples (Fig. 5a, b).
734 Therefore, our results indicate that the $\delta^{13}\text{C}$ composition of different long-chain *n*-alkane
735 homologues can be used to differentiate between xeric shrubland and savanna vegetation types
736 (Fig. 5a, b). As discussed above, grass and tree genera in savannas produce different relative
737 amounts of the *n*-C₂₉ and *n*-C₃₃. This leads to overall higher values for the grass-dominated $\delta^{13}\text{C}$
738 C₃₃ and higher $\delta^{13}\text{C}$ C₃₃₋₂₉ values in savanna samples (Fig. 5a). The lower $\delta^{13}\text{C}$ C₃₃₋₂₉ values in
739 Caatinga samples can be explained along similar lines. First, arid shrub and succulent species
740 synthesize *n*-alkanes with highly variable distributions, but overall tend to have longer chain-
741 length than C₃ trees (Boom et al., 2014; Carr et al., 2014; Feakins & Sessions, 2010). Thereby,
742 the mixing of material from different grass, shrub and succulent sources is not affecting specific
743 homologues as in savannas (Fig. 5a, b). Second, the differences in $\delta^{13}\text{C}$ composition of leaf-
744 waxes from different plant taxa are likely also less pronounced than between grasses and trees
745 found in Cerrado savanna. C₃ shrubs have elevated $\delta^{13}\text{C}$ composition due to aridity (Boom et al.,
746 2014) and succulents using CAM carbon fixation also feature $\delta^{13}\text{C}$ values that are between C₄
747 grass and C₃ tree endmembers (Messerschmid et al., 2021). The mixing of different Caatinga
748 sources therefore does not lead to the large differences between $\delta^{13}\text{C}$ C₃₃ and $\delta^{13}\text{C}$ C₂₉ observed
749 for the savanna settings, but to more uniform values (Fig. 5a).

750 While long-chain *n*-alkanes feature marked differences in $\delta^{13}\text{C}$ C₃₃₋₂₉ or $\delta^{13}\text{C}$ C₃₁₋₂₉ among
751 different vegetation types, long-chain fatty acids have a relatively homogeneous isotope
752 distribution, and the difference in $\delta^{13}\text{C}$ composition is consistent among the studied vegetation
753 types (Fig. 5c, d). An exception to this feature is the Llanos savanna samples, which show the
754 overall lowest $\delta^{13}\text{C}$ C₃₀₋₂₄ and $\delta^{13}\text{C}$ C₂₈₋₂₄ values. Since this is only observed in a very local set of
755 samples, the usefulness of this pattern would need further testing in larger sample sets.

756

757 **4.4.2. Comparison to tropical vegetation of other continents**

758 To expand the applicability of our findings on the differentiation of savannas and xeric
759 shrublands, we also analyzed previously published $\delta^{13}\text{C}$ C₃₃₋₂₉ data from Africa and tropical
760 South and Central America. As studies often report single homologue or pooled values, there is

761 only limited data on $\delta^{13}\text{C}$ C_{33} from soils available, especially from xeric shrublands (Fig. 8a).
762 Given this dearth of $\delta^{13}\text{C}$ C_{33} data, we also compiled $\delta^{13}\text{C}$ C_{31-29} data which showed a similar,
763 though muted pattern than $\delta^{13}\text{C}$ C_{33-29} in our data set (Fig. 5d).

764 In South and Central America, multi-homologue long-chain *n*-alkane data has been published on
765 soils from mountainous areas in Central America that covered tropical rainforests, dry forests
766 and tropical coniferous forests (Douglas et al., 2012), while another study exclusively covered
767 soils from the Amazon rainforest (Wu et al., 2019). In Africa, Schwab et al. (2015) provided *n*-
768 alkane $\delta^{13}\text{C}$ along a transect in Cameroon that covered forests, savanna and xeric shrubland
769 areas, while D. Zhang et al. (2021) covered savannas from the eastern African Serengeti and
770 Magill et al. (2019) also reported data from eastern Africa and South Africa. There has been an
771 extensive study on the major southwest African vegetation types, including the Nama Karoo and
772 Succulent Karoo xeric shrublands (Herrmann et al., 2016), which only reported $\delta^{13}\text{C}$ C_{29} and
773 $\delta^{13}\text{C}$ C_{31} values.

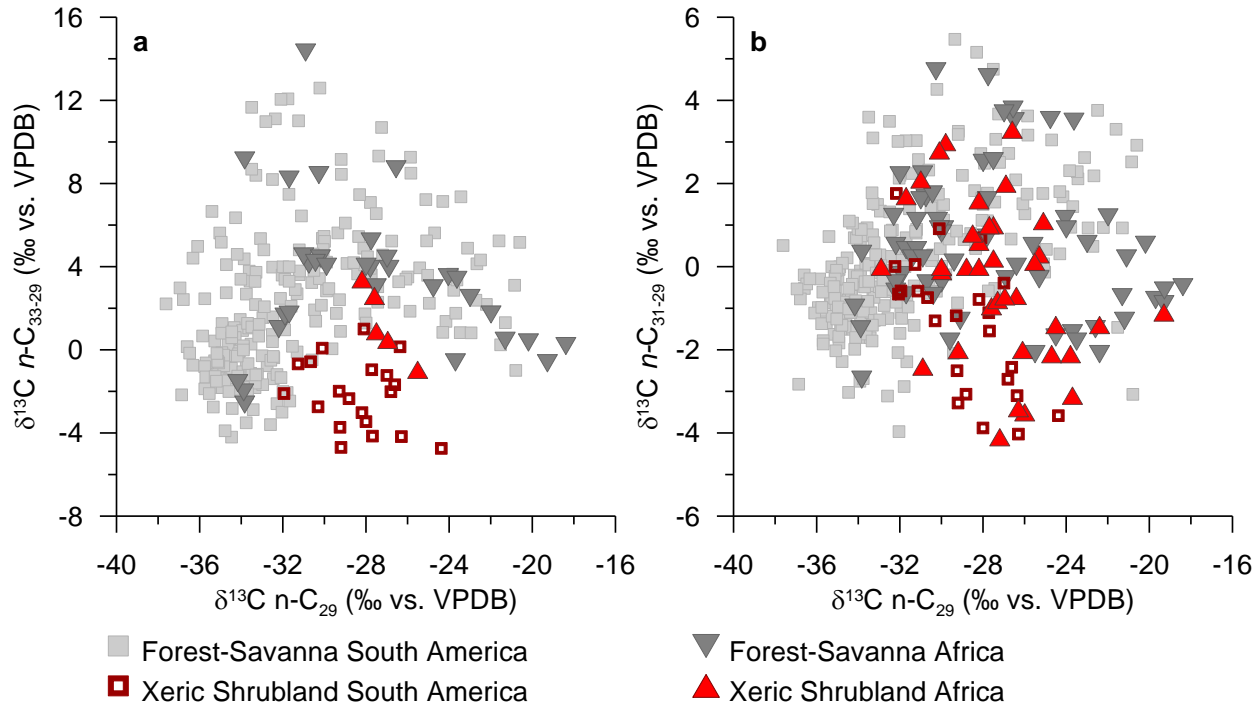
774 The $\delta^{13}\text{C}$ C_{33-29} trends in the forest-savanna continuum show lower values for forest and open
775 grass-dominated endmembers, while mixed savannas show higher values (Fig. 8a). The
776 magnitude of the increase in $\delta^{13}\text{C}$ C_{33-29} is comparable for African and South American savannas
777 (Fig. 8a). The shrublands also show consistently lower $\delta^{13}\text{C}$ C_{33-29} values in both South America
778 and Africa (Fig. 8a). $\delta^{13}\text{C}$ C_{31-29} trends also show comparable values for Africa and South
779 America and the lowest values in shrubland samples (Fig. 8b). There is however substantial
780 overlap between savanna and shrubland samples that limits the usefulness of $\delta^{13}\text{C}$ C_{31-29}
781 compared $\delta^{13}\text{C}$ C_{33-29} in differentiating between these vegetation types (Fig. 8b).

782 Our compilation shows that $\delta^{13}\text{C}$ C_{33-29} can be used to differentiate xeric shrubland and savannas
783 in the major tropical and subtropical areas of Africa and America, despite the different
784 evolutionary history and vegetation structure (Simon et al., 2009). The similarity of the patterns
785 between African and American savannas suggests that the savanna structure and species
786 diversity are not important for $\delta^{13}\text{C}$ C_{33-29} as long as there is a mixture of C_3 tree species with
787 their strongly dominant *n*- C_{29} production with C_4 grasses yielding modestly higher proportions in
788 *n*- C_{33} .

789

790 The isotopic offset between chain lengths are preserved through incorporation into soils in this
791 South American study (Fig. 6f) and there is also evidence from Africa that the isotope

792 distribution among homologues is retained through aerial and fluvial transport to marine
 793 deposition areas (Magill et al., 2019). Hence, there is promise for broad application of $\delta^{13}\text{C}$ C_{33-29}
 794 as a conservative tracer to differentiate between savannas and xeric shrublands in tropical soils
 795 and sediments of lakes and marine settings.



798 **Figure 8.** Stable carbon isotope composition ($\delta^{13}\text{C}$) variability among different n -alkane
 799 homologues in tropical vegetation types. a) $\delta^{13}\text{C}$ C_{33-29} in tropical vegetation types of Central-
 800 and South America (Douglas et al., 2012; Wu et al., 2019), as well as Africa (Magill et al., 2019;
 801 Schwab et al., 2015; D. Zhang et al., 2021). b) $\delta^{13}\text{C}$ C_{31-29} in tropical vegetation types of Central-
 802 and South America (Douglas et al., 2012; Wu et al., 2019), as well as Africa (Herrmann et al.,
 803 2016; Magill et al., 2019; Schwab et al., 2015; D. Zhang et al., 2021). All data were corrected for
 804 the Suess-effect.

805

806 4.5. Local variability

807 To study the variability of plant wax and $\delta^{13}\text{C}$ OC values at each site, we analyzed multiple
 808 (usually 5) samples per site. For mixed Cerrado types, we collected samples in the vicinity of
 809 trees and shrubs as well as in grass-dominated locations (Fig. 1c).

810 For $\delta^{13}\text{C}$ OC and the $\delta^{13}\text{C}$ composition of the different studied plant-wax homologues, we find
811 variability is greatest for mixed savanna sites, while forests show the lowest variability. The most
812 open vegetation types show intermediate values (Fig. 7a, c, e). A similar pattern is found for $\delta^{13}\text{C}$
813 C_{33-29} both on a sample specific level and averaged over each site (Fig. 7b, 8a). The main
814 contrast between the $\delta^{13}\text{C}$ C_{33-29} and the pattern of bulk $\delta^{13}\text{C}$ and plant wax $\delta^{13}\text{C}$ variability is
815 found in Caatinga shrublands. While $\delta^{13}\text{C}$ C_{33-29} values are close to zero, $\delta^{13}\text{C}$ OC variability is
816 similarly elevated in Caatinga shrublands and Cerrado savannas. While the causes for the
817 discrepancy in $\delta^{13}\text{C}$ C_{33-29} between Caatinga and Cerrado are already discussed above, the lack of
818 such a pattern in the variability of $\delta^{13}\text{C}$ OC and site-specific *n*-alkane and fatty acid $\delta^{13}\text{C}$ likely
819 arises from the considerable variety of $\delta^{13}\text{C}$ values found in different shrubland plants (Boom et
820 al., 2014; Messerschmid et al., 2021).

821

822 **5. Conclusions**

823 We studied the $\delta^{13}\text{C}$ composition of plant-wax long-chain *n*-alkanes and long-chain fatty acids in
824 soils and litter from the major biomes of tropical South America, with the objective to further
825 develop understanding of these proxies for vegetation reconstructions. Our results show that the
826 relative distribution of plant wax compounds (with the exception of long-chain *n*-alkanes $\geq n$ -
827 C_{29}) is detectably altered by microbial overturning in soils under open vegetation types. This
828 indicates that the relative distribution of plant wax abundances is not a suitable tool for
829 reconstructions of past vegetation in tropical South America. Conversely, isotope values remain
830 relatively stable during incorporation into soils. Tropical rainforest soils show $\delta^{13}\text{C}$ OC and plant
831 wax $\delta^{13}\text{C}$ compositions are within a narrow range, allowing the detection of even minor
832 occurrences of open vegetation. The most open vegetation types have the highest $\delta^{13}\text{C}$ values,
833 faithfully recording the increased abundance of grasses using the C_4 metabolism. The mixed
834 Cerrado savannas and the Caatinga shrublands show comparable $\delta^{13}\text{C}$ values, even though they
835 are distinctly different vegetation types growing under different climates. To differentiate
836 between the Cerrado savannas and the xeric Caatinga shrublands, we use the $\delta^{13}\text{C}$ composition of
837 long-chain *n*-alkane homologues of different chain-lengths. While savanna vegetation types
838 typically feature lower $\delta^{13}\text{C}$ values for the *n*- C_{29} homologue than for the *n*- C_{33} homologue,
839 Caatinga shrublands show consistent values for all homologues. We further compare our results
840 with published data from African savannas and xeric shrublands. We find that the $\delta^{13}\text{C}$

841 composition among different *n*-alkane homologues in Africa and tropical South America show
842 the same trends in the forest-savanna continuum and also in xeric shrublands. Likewise, the
843 relative distribution of plant waxes among different vegetation types is also consistent between
844 Africa and tropical South America. Both observations indicate a remarkable consistency despite
845 the different vegetation structure and evolutionary history of the savanna biomes of Africa and
846 South America. Overall, our study of tropical South American plant wax carbon isotopes
847 demonstrates that multiple plant wax homologues can be used to gain more detailed information
848 on past vegetation than obtained from single homologue analysis or the averaging of multiple
849 homologues into a single value.

850

851 **Acknowledgments**

852 This project was funded by a Swiss National Science Foundation (SNF) mobility fellowship
853 (grant P400P2_183856) to CH, supporting fieldwork and the postdoctoral researcher. Laboratory
854 analyses were supported by funding from University of Southern California and the Women in
855 Science and Engineering Program to SF. We acknowledge undergraduate laboratory assistants at
856 USC: Betlehem Assefa, Jonnie Dolan, Lindsay Luchinsky, Dea Kurti, Christopher Rincon and
857 Sharon Tu. Soils were imported under USDA Permit P330-19-00164 to SF. Fieldwork in the
858 eastern Amazon was funded by FAPESP (grant 2016/02656-9). DJB was financially supported
859 by the São Paulo Research Foundation (FAPESP) (grants 2019/24977-0 and 2022/06440-1).
860 CMC acknowledges the financial support from FAPESP (grants 2018/15123-4 and 2019/24349-
861 9), CNPq (grant 312458/2020-7), and the Alfred Wegener Institute for Polar and Marine
862 Research. AOS thanks the financial support from FAPESP (grant 2018/23899-2) and CNPq
863 (grant 307179/2021-4). TKA acknowledges the financial support from FAPESP (grants
864 2019/19948-0 and 2021/13129-8). VRM thanks the financial support from FAPESP (grant
865 2022/02957-0) and Serrapilheira (Serra R-2012-38252)

866

867 **Open Research**

868

869 The plant wax data presented in the study is available at zenodo.org via
870 <https://zenodo.org/doi/10.5281/zenodo.10214559> (Häggi, Bertassoli, et al., 2023).

871

872 **References**

- 873 Adler, D., & Kelly, S. T. (2019). vioplot: violin plot. R package version 0.3.4
 874 <https://github.com/TomKellyGenetics/vioplot>.
- 875 Almendros, G., Sanz, J., & Velasco, F. (1996). Signatures of lipid assemblages in soils under continental
 876 Mediterranean forests. *European Journal of Soil Science*, *47*(2), 183-196. doi:10.1111/j.1365-
 877 2389.1996.tb01389.x
- 878 Bertassoli, D. J., Häggi, C., Chiessi, C. M., Schefuß, E., Hefter, J., Akabane, T. K., & Sawakuchi, A. O. (2022).
 879 Controls on the distributions of GDGTs and n-alkane isotopic compositions in sediments of the Amazon
 880 River Basin. *Chemical Geology*, *594*, 120777. doi:10.1016/j.chemgeo.2022.120777
- 881 Bertassoli, D. J., Sawakuchi, A. O., Chiessi, C. M., Schefuß, E., Hartmann, G. A., Häggi, C., et al. (2019).
 882 Spatiotemporal Variations of Riverine Discharge Within the Amazon Basin During the Late Holocene
 883 Coincide With Extratropical Temperature Anomalies. *Geophysical Research Letters*, *46*(15), 9013-9022.
 884 doi:10.1029/2019GL082936
- 885 Blydenstein, J. (1967). Tropical Savanna Vegetation of the Llanos of Colombia. *Ecology*, *48*(1), 1-15.
 886 doi:10.2307/1933412
- 887 Boom, A., Carr, A. S., Chase, B. M., Grimes, H. L., & Meadows, M. E. (2014). Leaf wax n-alkanes and $\delta^{13}\text{C}$ values
 888 of CAM plants from arid southwest Africa. *Organic Geochemistry*, *67*, 99-102.
 889 doi:10.1016/j.orggeochem.2013.12.005
- 890 Brienen, R. J. W., Phillips, O. L., Feldpausch, T. R., Gloor, E., Baker, T. R., Lloyd, J., et al. (2015). Long-term
 891 decline of the Amazon carbon sink. *Nature*, *519*(7543), 344-348. Letter. doi:10.1038/nature14283
- 892 Brittingham, A., Hren, M. T., & Hartman, G. (2017). Microbial alteration of the hydrogen and carbon isotopic
 893 composition of n-alkanes in sediments. *Organic Geochemistry*, *107*, 1-8.
 894 doi:10.1016/j.orggeochem.2017.01.010
- 895 Bull, I. D., Bergen, P. F. v., Nott, C. J., Poulton, P. R., & Evershed, R. P. (2000). Organic geochemical studies of
 896 soils from the Rothamsted classical experiments—V. The fate of lipids in different long-term experiments.
 897 *Organic Geochemistry*, *31*(5), 389-408. doi:10.1016/S0146-6380(00)00008-5
- 898 Bush, R. T., & McInerney, F. A. (2013). Leaf wax n-alkane distributions in and across modern plants: Implications
 899 for paleoecology and chemotaxonomy. *Geochimica Et Cosmochimica Acta*, *117*, 161-179.
 900 doi:10.1016/j.gca.2013.04.016
- 901 Bush, R. T., & McInerney, F. A. (2015). Influence of temperature and C4 abundance on n-alkane chain length
 902 distributions across the central USA. *Organic Geochemistry*, *79*, 65-73.
 903 doi:10.1016/j.orggeochem.2014.12.003
- 904 Carr, A. S., Boom, A., Grimes, H. L., Chase, B. M., Meadows, M. E., & Harris, A. (2014). Leaf wax n-alkane
 905 distributions in arid zone South African flora: Environmental controls, chemotaxonomy and
 906 palaeoecological implications. *Organic Geochemistry*, *67*, 72-84. doi:10.1016/j.orggeochem.2013.12.004
- 907 Ceccopieri, M., Scofield, A. L., Almeida, L., Araújo, M. P., Hamacher, C., Farias, C. O., et al. (2021). Carbon
 908 isotopic composition of leaf wax n-alkanes in mangrove plants along a latitudinal gradient in Brazil.
 909 *Organic Geochemistry*, *161*, 104299. doi:10.1016/j.orggeochem.2021.104299
- 910 Cerling, T. E., Harris, J. M., MacFadden, B. J., Leakey, M. G., Quade, J., Eisenmann, V., & Ehleringer, J. R. (1997).
 911 Global vegetation change through the Miocene/Pliocene boundary. *Nature*, *389*, 153. doi:10.1038/38229
- 912 Cerling, T. E., Wynn, J. G., Andanje, S. A., Bird, M. I., Korir, D. K., Levin, N. E., et al. (2011). Woody cover and
 913 hominin environments in the past 6 million years. *Nature*, *476*, 51. doi:10.1038/nature10306
- 914 Chen, G., Li, X., Tang, X., Qin, W., Liu, H., Zech, M., & Auerswald, K. (2022). Variability in pattern and hydrogen
 915 isotope composition ($\delta^2\text{H}$) of long-chain n-alkanes of surface soils and its relations to climate and
 916 vegetation characteristics: A meta-analysis. *Pedosphere*, *32*(3), 369-380. doi:10.1016/S1002-
 917 0160(21)60080-2
- 918 Chikaraishi, Y., & Naraoka, H. (2006). Carbon and hydrogen isotope variation of plant biomarkers in a plant–soil
 919 system. *Chemical Geology*, *231*(3), 190-202. doi:10.1016/j.chemgeo.2006.01.026
- 920 Collister, J. W., Rieley, G., Stern, B., Eglinton, G., & Fry, B. (1994). Compound-Specific Delta C-13 Analyses of
 921 leaf lipids from plants with differing carbon-dioxide metabolisms. *Org. Geochem.*, *21*(6-7), 619-627.
 922 doi:10.1016/0146-6380(94)90008-6

- 923 Cox, P. M., Pearson, D., Booth, B. B., Friedlingstein, P., Huntingford, C., Jones, C. D., & Luke, C. M. (2013).
 924 Sensitivity of tropical carbon to climate change constrained by carbon dioxide variability. *Nature*,
 925 *494*(7437), 341-344. doi:10.1038/nature11882
- 926 Cranwell, P. A. (1981). Diagenesis of free and bound lipids in terrestrial detritus deposited in a lacustrine sediment.
 927 *Org. Geochem.*, *3*, 79-89. doi:10.1016/0146-6380(81)90002-4
- 928 da Silva, J. M. C., & Bates, J. M. (2002). Biogeographic patterns and conservation in the South American Cerrado:
 929 A tropical Savanna hotspot. *Bioscience*, *52*(3), 225-233. doi:10.1641/0006-
 930 3568(2002)052[0225:BPACIT]2.0.CO;2
- 931 da Silva, J. M. C., & Lacher, T. E. (2020). Caatinga—South America. In M. I. Goldstein & D. A. DellaSala (Eds.),
 932 *Encyclopedia of the World's Biomes* (pp. 554-561). Oxford: Elsevier.
- 933 Dantas, V. D., & Pausas, J. G. (2013). The lanky and the corky: fire-escape strategies in savanna woody species.
 934 *Journal of Ecology*, *101*(5), 1265-1272. doi:10.1111/1365-2745.12118
- 935 De Azevedo, A. (1950). Regiões climato-botânicas do Brasil. *Anuário Brasileiro de Economia Florestal*, *11*, 201-
 936 232.
- 937 de Queiroz, L. P. (2006). The Brazilian Caatinga: phytogeographical patterns inferred from distribution data of the
 938 Leguminosae. In *Neotropical Savannas and Seasonally Dry Forests* (pp. 121-157): CRC Press.
- 939 Diefendorf, A. F., Mueller, K. E., Wing, S. L., Koch, P. L., & Freeman, K. H. (2010). Global patterns in leaf 13C
 940 discrimination and implications for studies of past and future climate. *Proceedings of the National
 941 Academy of Sciences*, *107*(13), 5738-5743. doi:10.1073/pnas.0910513107
- 942 Douglas, P. M. J., Pagani, M., Brenner, M., Hodell, D. A., & Curtis, J. H. (2012). Aridity and vegetation
 943 composition are important determinants of leaf-wax δD values in southeastern Mexico and Central
 944 America. *Geochimica Et Cosmochimica Acta*, *97*, 24-45. doi:10.1016/j.gca.2012.09.005
- 945 Eckmeier, E., & Wiesenberg, G. L. B. (2009). Short-chain n-alkanes (C16–20) in ancient soil are useful molecular
 946 markers for prehistoric biomass burning. *Journal of Archaeological Science*, *36*(7), 1590-1596.
 947 doi:10.1016/j.jas.2009.03.021
- 948 Edwards, E. J., Osborne, C. P., Strömberg, C. A. E., & Smith, S. A. (2010). The Origins of C4 Grasslands:
 949 Integrating Evolutionary and Ecosystem Science. *Science*, *328*(5978), 587-591.
 950 doi:10.1126/science.1177216
- 951 Eglinton, G., & Hamilton, R. J. (1967). Leaf epicuticular waxes. *Science*, *156*(3780), 1322-1335.
 952 doi:10.1126/science.156.3780.1322
- 953 Eiten, G. (1972). The cerrado vegetation of Brazil. *The Botanical Review*, *38*(2), 201-341. doi:10.1007/BF02859158
- 954 Faria, S. R., De La Rosa, J. M., Knicker, H., González-Pérez, J. A., Villaverde, J., & Keizer, J. J. (2015). Wildfire-
 955 induced alterations of topsoil organic matter and their recovery in Mediterranean eucalypt stands detected
 956 with biogeochemical markers. *European Journal of Soil Science*, *66*(4), 699-713. doi:10.1111/ejss.12254
- 957 Feakins, S. J., Levin, N. E., Liddy, H. M., Sieracki, A., Eglinton, T. I., & Bonnefille, R. (2013). Northeast African
 958 vegetation change over 12 m.y. *Geology*, *41*(3), 295-298. doi:10.1130/g33845.1
- 959 Feakins, S. J., Peters, T., Wu, M. S., Shenkin, A., Salinas, N., Girardin, C. A. J., et al. (2016). Production of leaf wax
 960 n-alkanes across a tropical forest elevation transect. *Organic Geochemistry*, *100*, 89-100.
 961 doi:10.1016/j.orggeochem.2016.07.004
- 962 Feakins, S. J., & Sessions, A. L. (2010). Crassulacean acid metabolism influences D/H ratio of leaf wax in succulent
 963 plants. *Organic Geochemistry*, *41*(12), 1269-1276. doi:10.1016/j.orggeochem.2010.09.007
- 964 Feakins, S. J., Wu, M. S., Ponton, C., Galy, V., & West, A. J. (2018). Dual isotope evidence for sedimentary
 965 integration of plant wax biomarkers across an Andes-Amazon elevation transect. *Geochimica Et
 966 Cosmochimica Acta*, *242*, 64-81. doi:10.1016/j.gca.2018.09.007
- 967 Ferreira, J. Q., Chiessi, C. M., Hirota, M., Oliveira, R. S., Prange, M., Häggi, C., et al. (2022). Changes in obliquity
 968 drive tree cover shifts in eastern tropical South America. *Quaternary Science Reviews*, *279*, 107402.
 969 doi:10.1016/j.quascirev.2022.107402
- 970 Ficken, K. J., Li, B., Swain, D. L., & Eglinton, G. (2000). An n-alkane proxy for the sedimentary input of
 971 submerged/floating freshwater aquatic macrophytes. *Organic Geochemistry*, *31*(7–8), 745-749.
 972 doi:10.1016/S0146-6380(00)00081-4
- 973 Fornace, K. L., Whitney, B. S., Galy, V., Huguen, K. A., & Mayle, F. E. (2016). Late Quaternary environmental
 974 change in the interior South American tropics: new insight from leaf wax stable isotopes. *Earth and
 975 Planetary Science Letters*, *438*, 75-85. doi:10.1016/j.epsl.2016.01.007
- 976 Garcin, Y., Schefuß, E., Schwab, V. F., Garreta, V., Gleixner, G., Vincens, A., et al. (2014). Reconstructing C3 and
 977 C4 vegetation cover using n-alkane carbon isotope ratios in recent lake sediments from Cameroon, Western
 978 Central Africa. *Geochimica Et Cosmochimica Acta*, *142*, 482-500. doi:10.1016/j.gca.2014.07.004

- 979 Goñi, M. A., Ruttner, K. C., & Eglinton, T. I. (1997). Sources and contribution of terrigenous organic carbon to
980 surface sediments in the Gulf of Mexico. *Nature*, 389, 275. doi:10.1038/38477
- 981 Goodland, R. (1971). A Physiognomic Analysis of the 'Cerrado' Vegetation of Central Brasil. *Journal of Ecology*,
982 59(2), 411-419. doi:10.2307/2258321
- 983 Häggi, C., Bertassoli, D. J., Akabane, T. K., So, R. T., Sawakuchi, A. O., Chiessi, C. M., et al. (2023). Plantwax
984 carbon isotope data from tropical South American surface soils [Data set]. Zenodo.
985 <https://doi.org/10.5281/zenodo.10214560>.
- 986 Häggi, C., Chiessi, C. M., Merkel, U., Mulitza, S., Prange, M., Schulz, M., & Schefuß, E. (2017). Response of the
987 Amazon rainforest to late Pleistocene climate variability. *Earth and Planetary Science Letters*, 479, 50-59.
988 doi:10.1016/j.epsl.2017.09.013
- 989 Häggi, C., Naafs, B. D. A., Silvestro, D., Bertassoli, D. J., Akabane, T. K., Mendes, V. R., et al. (2023). GDGT
990 distribution in tropical soils and its potential as a terrestrial paleothermometer revealed by Bayesian deep-
991 learning models. *Geochimica Et Cosmochimica Acta*, 362, 41-64. doi:j.gca.2023.09.014
- 992 Häggi, C., Pätzold, J., Bouillon, S., & Schefuß, E. (2021). Impact of selective degradation on molecular isotope
993 compositions in oxic and anoxic marine sediments. *Organic Geochemistry*, 153, 104192.
994 doi:10.1016/j.orggeochem.2021.104192
- 995 Häggi, C., Sawakuchi, A. O., Chiessi, C. M., Mulitza, S., Mollenhauer, G., Sawakuchi, H. O., et al. (2016). Origin,
996 transport and deposition of leaf-wax biomarkers in the Amazon Basin and the adjacent Atlantic.
997 *Geochimica Et Cosmochimica Acta*, 192, 149-165. doi:10.1016/j.gca.2016.07.002
- 998 Herrmann, N., Boom, A., Carr, A. S., Chase, B. M., Granger, R., Hahn, A., et al. (2016). Sources, transport and
999 deposition of terrestrial organic material: A case study from southwestern Africa. *Quaternary Science*
1000 *Reviews*, 149, 215-229. doi:10.1016/j.quascirev.2016.07.028
- 1001 Hirota, M., Holmgren, M., Van Nes, E. H., & Scheffer, M. (2011). Global Resilience of Tropical Forest and
1002 Savanna to Critical Transitions. *Science*, 334(6053), 232-235. doi:10.1126/science.1210657
- 1003 Hoyos, N., Correa-Metrio, A., Jaramillo, C., Villegas, J. C., & Escobar, J. (2022). Effects of consecutive dry and wet
1004 days on the forest-savanna boundary in north-west South America. *Global Ecology and Biogeography*,
1005 31(2), 347-361. doi:10.1111/geb.13432
- 1006 Huang, Y., Dupont, L., Sarnthein, M., Hayes, J. M., & Eglinton, G. (2000). Mapping of C4 plant input from North
1007 West Africa into North East Atlantic sediments. *Geochimica Et Cosmochimica Acta*, 64(20), 3505-3513.
1008 doi:10.1016/S0016-7037(00)00445-2
- 1009 Huang, Y., Eglinton, G., Ineson, P., Latter, P. M., Bol, R., & Harkness, D. D. (1997). Absence of carbon isotope
1010 fractionation of individual n-alkanes in a 23-year field decomposition experiment with *Calluna vulgaris*.
1011 *Organic Geochemistry*, 26(7), 497-501. doi:10.1016/S0146-6380(97)00027-2
- 1012 Huang, Y., Street-Perrott, F. A., Metcalfe, S. E., Brenner, M., Moreland, M., & Freeman, K. H. (2001). Climate
1013 Change as the Dominant Control on Glacial-Interglacial Variations in C3 and C4 Plant Abundance.
1014 *Science*, 293(5535), 1647-1651. doi:10.1126/science.1060143
- 1015 Jaramillo, C. (2023). The evolution of extant South American tropical biomes. *New Phytologist*, 239(2), 477-493.
1016 doi:10.1111/nph.18931
- 1017 Jenkins, C. N., Pimm, S. L., & Joppa, L. N. (2013). Global patterns of terrestrial vertebrate diversity and
1018 conservation. *Proceedings of the National Academy of Sciences*, 110(28), 2602-2610.
1019 doi:10.1073/pnas.1302251110
- 1020 Ji, Y., Mao, G., Wang, Y., & Bartlam, M. (2013). Structural insights into diversity and n-alkane biodegradation
1021 mechanisms of alkane hydroxylases. *Frontiers in microbiology*, 4. Review. doi:10.3389/fmicb.2013.00058
- 1022 Karger, D. N., Conrad, O., Böhner, J., Kawohl, T., Kreft, H., Soria-Auza, R. W., et al. (2017). Climatologies at high
1023 resolution for the earth's land surface areas. *Scientific Data*, 4(1), 170122. doi:10.1038/sdata.2017.122
- 1024 Kier, G., Kreft, H., Lee, T. M., Jetz, W., Ibsch, P. L., Nowicki, C., et al. (2009). A global assessment of endemism
1025 and species richness across island and mainland regions. *Proceedings of the National Academy of Sciences*,
1026 106(23), 9322-9327. doi:10.1073/pnas.0810306106
- 1027 Kohn, M. J. (2010). Carbon isotope compositions of terrestrial C3 plants as indicators of (paleo)ecology and
1028 (paleo)climate. *Proceedings of the National Academy of Sciences*, 107(46), 19691-19695.
1029 doi:10.1073/pnas.1004933107
- 1030 Kortschak, H. P., Hartt, C. E., & Burr, G. O. (1965). Carbon Dioxide Fixation in Sugarcane Leaves. *Plant*
1031 *Physiology*, 40(2), 209-213. doi:10.1104/pp.40.2.209
- 1032 Krull, E., Sachse, D., Mügler, I., Thiele, A., & Gleixner, G. (2006). Compound-specific $\delta^{13}\text{C}$ and $\delta^2\text{H}$ analyses of
1033 plant and soil organic matter: A preliminary assessment of the effects of vegetation change on ecosystem
1034 hydrology. *Soil Biology and Biochemistry*, 38(11), 3211-3221. doi:10.1016/j.soilbio.2006.04.008

- 1035 Lehmann, C. E. R., Anderson, T. M., Sankaran, M., Higgins, S. I., Archibald, S., Hoffmann, W. A., et al. (2014).
 1036 Savanna Vegetation-Fire-Climate Relationships Differ Among Continents. *Science*, *343*(6170), 548-552.
 1037 doi:10.1126/science.1247355
- 1038 Liu, J., & An, Z. (2020). Leaf wax n-alkane carbon isotope values vary among major terrestrial plant groups:
 1039 Different responses to precipitation amount and temperature, and implications for paleoenvironmental
 1040 reconstruction. *Earth-Science Reviews*, *202*, 103081. doi:10.1016/j.earscirev.2020.103081
- 1041 Liu, J., Zhao, J., He, D., Huang, X., Jiang, C., Yan, H., et al. (2022). Effects of plant types on terrestrial leaf wax
 1042 long-chain n-alkane biomarkers: Implications and paleoapplications. *Earth-Science Reviews*, *235*, 104248.
 1043 doi:10.1016/j.earscirev.2022.104248
- 1044 Liu, W., Huang, Y., An, Z., Clemens, S. C., Li, L., Prell, W. L., & Ning, Y. (2005). Summer monsoon intensity
 1045 controls C4/C3 plant abundance during the last 35 ka in the Chinese Loess Plateau: Carbon isotope
 1046 evidence from bulk organic matter and individual leaf waxes. *Palaeogeography, Palaeoclimatology,*
 1047 *Palaeoecology*, *220*(3), 243-254. doi:10.1016/j.palaeo.2005.01.001
- 1048 Lloyd, J., Bird, M. I., Vellen, L., Miranda, A. C., Veenendaal, E. M., Djagbletey, G., et al. (2008). Contributions of
 1049 woody and herbaceous vegetation to tropical savanna ecosystem productivity: a quasi-global estimate†.
 1050 *Tree Physiology*, *28*(3), 451-468. doi:10.1093/treephys/28.3.451
- 1051 Magill, C. R., Ashley, G. M., & Freeman, K. H. (2013). Ecosystem variability and early human habitats in eastern
 1052 Africa. *Proceedings of the National Academy of Sciences*, *110*(4), 1167-1174.
 1053 doi:10.1073/pnas.1206276110
- 1054 Magill, C. R., Eglinton, G., & Eglinton, T. I. (2019). Isotopic variance among plant lipid homologues correlates with
 1055 biodiversity patterns of their source communities. *Plos One*, *14*(2), e0212211.
 1056 doi:10.1371/journal.pone.0212211
- 1057 Martinelli, L. A., Nardoto, G. B., Soltangheisi, A., Reis, C. R. G., Abdalla-Filho, A. L., Camargo, P. B., et al.
 1058 (2020). Determining ecosystem functioning in Brazilian biomes through foliar carbon and nitrogen
 1059 concentrations and stable isotope ratios. *Biogeochemistry*. doi:10.1007/s10533-020-00714-2
- 1060 Messerschmid, T. F. E., Wehling, J., Bobon, N., Kahmen, A., Klak, C., Los, J. A., et al. (2021). Carbon isotope
 1061 composition of plant photosynthetic tissues reflects a Crassulacean Acid Metabolism (CAM) continuum in
 1062 the majority of CAM lineages. *Perspectives in Plant Ecology, Evolution and Systematics*, *51*, 125619.
 1063 doi:10.1016/j.ppees.2021.125619
- 1064 Minasny, B., Malone, B. P., McBratney, A. B., Angers, D. A., Arrouays, D., Chambers, A., et al. (2017). Soil
 1065 carbon 4 per mille. *Geoderma*, *292*, 59-86. doi:10.1016/j.geoderma.2017.01.002
- 1066 Mulitza, S., Chiessi, C. M., Schefuß, E., Lippold, J., Wichmann, D., Antz, B., et al. (2017). Synchronous and
 1067 proportional deglacial changes in Atlantic meridional overturning and northeast Brazilian precipitation.
 1068 *Paleoceanography*, *32*(6), 622-633. doi:10.1002/2017PA003084
- 1069 Nguyen Tu, T. T., Egasse, C., Zeller, B., Bardoux, G., Biron, P., Ponge, J.-F., et al. (2011). Early degradation of
 1070 plant alkanes in soils: A litterbag experiment using ¹³C-labelled leaves. *Soil Biology and Biochemistry*,
 1071 *43*(11), 2222-2228. doi:10.1016/j.soilbio.2011.07.009
- 1072 O'Leary, M. H. (1981). Carbon isotope fractionation in plants. *Phytochemistry*, *20*(4), 553-567. doi:10.1016/0031-
 1073 9422(81)85134-5
- 1074 Ofiti, N., Zosso, C., Soong, J., Solly, E., Torn, M., Wiesenberg, G., & Schmidt, M. (2021). Warming promotes loss
 1075 of subsoil carbon through accelerated degradation of plant-derived organic matter. *Soil Biology and*
 1076 *Biochemistry*, *156*, 108185. doi:10.1016/j.soilbio.2021.108185
- 1077 Oliveira-Filho, A. T., & Fontes, M. A. L. (2000). Patterns of Floristic Differentiation among Atlantic Forests in
 1078 Southeastern Brazil and the Influence of Climate1. *Biotropica*, *32*(4b), 793-810. doi:10.1111/j.1744-
 1079 7429.2000.tb00619.x
- 1080 Olson, D. M., Dinerstein, E., Wikramanayake, E. D., Burgess, N. D., Powell, G. V. N., Underwood, E. C., et al.
 1081 (2001). Terrestrial ecoregions of the worlds: A new map of life on Earth. *Bioscience*, *51*(11), 933-938.
 1082 doi:10.1641/0006-3568(2001)051[0933:teotwa]2.0.co;2
- 1083 Pivello, V. R. (2011). The use of fire in the Cerrado and Amazonian rainforest of Brazil: Past and present. *Fire*
 1084 *Ecology*, *7*(1), 24-39. doi:10.4996/fireecology.0701024
- 1085 R_Core_Team. (2022). R: A Language and Environment for Statistical Computing. Vienna, Austria: R Foundation
 1086 for Statistical Computing. Retrieved from <https://www.R-project.org>
- 1087 Reis, L. S., Bouloubassi, I., Mendez-Millan, M., Guimarães, J. T. F., de Araújo Romeiro, L., Sahoo, P. K., &
 1088 Pessenda, L. C. R. (2022). Hydroclimate and vegetation changes in southeastern Amazonia over the past
 1089 ~25,000 years. *Quaternary Science Reviews*, *284*, 107466. doi:10.1016/j.quascirev.2022.107466

- 1090 Rieley, G., Collier, R. J., Jones, D. M., Eglinton, G., Eakin, P. A., & Fallick, A. E. (1991). Sources of sedimentary
 1091 lipids deduced from stable carbon-isotope analyses of individual compounds. *Nature*, *352*(6334), 425-427.
 1092 10.1038/352425a0. doi:10.1038/352425a0
- 1093 Rommerskirchen, F., Eglinton, G., Dupont, L., Güntner, U., Wenzel, C., & Rullkötter, J. (2003). A north to south
 1094 transect of Holocene southeast Atlantic continental margin sediments: Relationship between aerosol
 1095 transport and compound-specific $\delta^{13}\text{C}$ land plant biomarker and pollen records. *Geochemistry, Geophysics,*
 1096 *Geosystems*, *4*(12), 1101–1128. doi:10.1029/2003GC000541
- 1097 Rommerskirchen, F., Plader, A., Eglinton, G., Chikaraishi, Y., & Rullkötter, J. (2006). Chemotaxonomic
 1098 significance of distribution and stable carbon isotopic composition of long-chain alkanes and alkan-1-ols in
 1099 C-4 grass waxes. *Organic Geochemistry*, *37*(10), 1303-1332. doi:10.1016/j.orggeochem.2005.12.013
- 1100 Ruggiero, P. G. C., Batalha, M. A., Pivello, V. R., & Meirelles, S. T. (2002). Soil-vegetation relationships in cerrado
 1101 (Brazilian savanna) and semideciduous forest, Southeastern Brazil. *Plant Ecology*, *160*(1), 1-16.
 1102 doi:10.1023/A:1015819219386
- 1103 Salati, E., Dall'Olio, A., Matsui, E., & Gat, J. R. (1979). Recycling of water in the Amazon Basin: An isotopic study.
 1104 *Water Resources Research*, *15*(5), 1250-1258. doi:10.1029/WR015i005p01250
- 1105 Sarangi, V., Roy, S., & Sanyal, P. (2022). Effect of burning on the distribution pattern and isotopic composition of
 1106 plant biomolecules: Implications for paleoecological studies. *Geochimica Et Cosmochimica Acta*, *318*, 305-
 1107 327. doi:10.1016/j.gca.2021.12.003
- 1108 Schefuß, E., Schouten, S., & Schneider, R. R. (2005). Climatic controls on central African hydrology during the past
 1109 20,000 years. *Nature*, *437*(7061), 1003-1006. doi:10.1038/nature03945
- 1110 Schwab, V. F., Garcin, Y., Sachse, D., Todou, G., Séné, O., Onana, J.-M., et al. (2015). Effect of aridity on $\delta^{13}\text{C}$
 1111 and δD values of C3 plant- and C4 graminoid-derived leaf wax lipids from soils along an environmental
 1112 gradient in Cameroon (Western Central Africa). *Organic Geochemistry*, *78*, 99-109.
 1113 doi:10.1016/j.orggeochem.2014.09.007
- 1114 Sexton, J. O., Song, X.-P., Feng, M., Noojipady, P., Anand, A., Huang, C., et al. (2013). Global, 30-m resolution
 1115 continuous fields of tree cover: Landsat-based rescaling of MODIS vegetation continuous fields with lidar-
 1116 based estimates of error. *International Journal of Digital Earth*, *6*(5), 427-448.
 1117 doi:10.1080/17538947.2013.786146
- 1118 Simon, M. F., Grether, R., de Queiroz, L. P., Skema, C., Pennington, R. T., & Hughes, C. E. (2009). Recent
 1119 assembly of the Cerrado, a neotropical plant diversity hotspot, by in situ evolution of adaptations to fire.
 1120 *Proceedings of the National Academy of Sciences*, *106*(48), 20359-20364. doi:10.1073/pnas.0903410106
- 1121 Slack, C. R., & Hatch, M. D. (1967). Comparative studies on the activity of carboxylases and other enzymes in
 1122 relation to the new pathway of photosynthetic carbon dioxide fixation in tropical grasses. *The Biochemical*
 1123 *journal*, *103*(3), 660-665. doi:10.1042/bj1030660
- 1124 Stockmann, U., Padarian, J., McBratney, A., Minasny, B., de Brogniez, D., Montanarella, L., et al. (2015). Global
 1125 soil organic carbon assessment. *Global Food Security*, *6*, 9-16. doi:10.1016/j.gfs.2015.07.001
- 1126 Tu, T. T. N., Derenne, S., Largeau, C., Bardoux, G., & Mariotti, A. (2004). Diagenesis effects on specific carbon
 1127 isotope composition of plant n-alkanes. *Organic Geochemistry*, *35*(3), 317-329.
 1128 doi:10.1016/j.orggeochem.2003.10.012
- 1129 Vogts, A., Moossen, H., Rommerskirchen, F., & Rullkötter, J. (2009). Distribution patterns and stable carbon
 1130 isotopic composition of alkanes and alkan-1-ols from plant waxes of African rain forest and savanna C3
 1131 species. *Organic Geochemistry*, *40*(10), 1037-1054. doi:10.1016/j.orggeochem.2009.07.011
- 1132 Wu, M. S., Feakins, S. J., Martin, R. E., Shenkin, A., Bentley, L. P., Blonder, B., et al. (2017). Altitude effect on leaf
 1133 wax carbon isotopic composition in humid tropical forests. *Geochimica Et Cosmochimica Acta*, *206*, 1-17.
 1134 doi:10.1016/j.gca.2017.02.022
- 1135 Wu, M. S., West, A. J., & Feakins, S. J. (2019). Tropical soil profiles reveal the fate of plant wax biomarkers during
 1136 soil storage. *Organic Geochemistry*, *128*, 1-15. doi:10.1016/j.orggeochem.2018.12.011
- 1137 Yang, C.-K., Huang, B.-H., Ho, S.-W., Huang, M.-Y., Wang, J.-C., Gao, J., & Liao, P.-C. (2018). Molecular genetic
 1138 and biochemical evidence for adaptive evolution of leaf abaxial epicuticular wax crystals in the genus
 1139 *Lithocarpus* (Fagaceae). *BMC Plant Biology*, *18*(1), 196. doi:10.1186/s12870-018-1420-4
- 1140 Yang, D., & Bowen, G. J. (2022). Integrating plant wax abundance and isotopes for paleo-vegetation and
 1141 paleoclimate reconstructions: a multi-source mixing model using a Bayesian framework. *Clim. Past*,
 1142 *18*(10), 2181-2210. doi:10.5194/cp-18-2181-2022
- 1143 Zemp, D. C., Schleussner, C.-F., Barbosa, H. M. J., Hirota, M., Montade, V., Sampaio, G., et al. (2017). Self-
 1144 amplified Amazon forest loss due to vegetation-atmosphere feedbacks. *Nature Communications*, *8*(1),
 1145 14681. doi:10.1038/ncomms14681

- 1146 Zhang, D., Beverly, E. J., Levin, N. E., Vidal, E., Matia, Y., & Feakins, S. J. (2021). Carbon isotopic composition of
1147 plant waxes, bulk organics and carbonates from soils of the Serengeti grasslands. *Geochimica Et*
1148 *Cosmochimica Acta*, *311*, 316-331. doi:10.1016/j.gca.2021.07.005
1149 Zhang, Y., Zheng, M., Meyers, P. A., & Huang, X. (2017). Impact of early diagenesis on distributions of Sphagnum
1150 n-alkanes in peatlands of the monsoon region of China. *Organic Geochemistry*, *105*, 13-19.
1151 doi:10.1016/j.orggeochem.2016.12.007

1152